Micro-seismic Observations in Leeu Gamka, Karoo, South Africa.

A thesis submitted for the degree of Master of Science in the Department of Geological Sciences at the University of Cape Town, South Africa

Supervisors: Richard Kahle

Beth Kahle

Melody Fynn

February 2018

Declaration

By submitting this thesis electronically, I declare that:

1) I know that plagiarism is wrong. Plagiarism is to use another's work and pass it off as my own.
2) The entirety of the work contained therein is my own work, written in my own words.
3) I have used the Harvard convention for citation and referencing. Each contribution to and quotation in this thesis from the work(s) of other people has been attributed and has been cited and referenced.
4) I have not allowed, and will not allow, anyone to copy my work with the intention of passing it off as his or her own work.

Signed by candidate

Melody Fynn (Student number: FYNMEL001)
Date: 19 February 2018

Abstract

This thesis documents a microseismicity study in the interior of South Africa. The study area is centred on Leeu Gamka in the Western Cape province, a tectonically stable intraplate setting and is therefore expected to be seismically quiet. The International Seismological Centre (ISC) catalogue reported localised anomalous seismicity in the region between 2007 and 2013 with local magnitudes up to 4.5. The short apparent duration and time history of this anomalous reported seismicity is likely a reporting artefact. An array of 23 geophones was deployed for three months (March – June) in 2015, covering an area of 60 km × 65 km centred on the zone of anomalous seismicity. Using this array, I identified a total of 106 earthquakes over this period, with almost all events clustering in a surprisingly small area (75% of the epicentres fall within a one square kilometre block). Double-difference relocation resolved the hypocentres onto a structure with an apparent NW – SE orientation, consistent with large-scale fabric that can be recognised in satellite imagery. The focal mechanisms display strike-slip faulting with the fault plane likely in a NW – SE orientation, consistent with the distribution of the earthquakes. The velocity model was tested by varying the thickness of the Karoo supergroup to investigate the sensitivity of the depths of the earthquakes. An average hypocentral depth of approximately 6 km was calculated for the earthquakes, assuming a depth to the base of the Karoo of 5km. This places the earthquakes just below the base of the Karoo in the Cape Supergroup. The magnitudes of the earthquakes recorded range from -1.5$<M_{\mathrm{L}}<$0.4, with a magnitude of completeness of -0.8, and follow a Gutenberg-Richter distribution with the b-value range of 1.23 – 2.07 calculated within a 90 % confidence range. The presence of such a structure has implications for shale gas exploration in that wastewater pumping in an area with active faulting could trigger larger and more frequent earthquakes, as seen in case studies in the central states of America, in particular, Oklahoma.

Acknowledgements

I would like to thank Chris Hartnady whose enthusiastic interest in seismicity in the Karoo, inspired this research. To my supervisors, Beth and Richard, thank you for your incredible guidance and support throughout the process of producing this thesis. I am eternally grateful for your motivation, encouragement and constant reminders of the importance of my research. Thank you for not allowing me to submit anything that was less than my absolute best effort. To my family who constantly listened and supported me through all my moments of self-doubt and complaints of exhaustion and offering refuge when things got tough. Thank you to my father, who tirelessly listened to my ideas and was always up to engaging in great discussions. To my partner for supporting and encouraging me and putting up with many days of varying moods. Your motivation, love and constant support I could not have done without. To the Leeu Gamka farmers, to whom I dedicate this thesis, none of this research would have been possible without your permission and support. Thank you for the tea and rusks and interesting conversations that made me fall in love with the Karoo, I thank you. Finally, thanks to the NRF and UCT for funding most of my research activities and affording me the opportunity to travel to Europe for the first time to present my research at the European Geosciences Union in Vienna.

Contents

List of Figures

List of Tables

"Perhaps we will be less embarrassed in the future
than we have been in the recent past by large earthquakes
that occurred on faults that were unknown or unappreciated
at the time, but most of which could have been identified beforehand,
given our better understanding of what to look for."

JAMES JACKSON

1 Introduction

The aim of this study is to investigate the micro-seismicity in a region where anomalous seismicity was recorded during the period between 2007 – 2013. The study area is located in an intraplate region, which is expected to be tectonically stable (Green and Bloch, 1971). Earthquakes are usually confined to narrow zones (Figure 1.1) at the plate boundaries (Isacks et al., 1968) because the large relative motion between the bounding plates results in a build-up of strain that is released over a small area (Byerlee, 1966; Byerlee and Brace, 1968). The essential concept of plate tectonics is that stress builds up on faults over time, until the frictional strength of the clamping forces holding the fault together is exceeded, releasing energy in the form of an earthquake (Anderson, 1951). South Africa, and in particular Leeu Gamka, is located far from plate boundaries. Most of the seismicity recorded in South Africa is mining-related, particularly in the north-east of the country. Occasionally, clusters of earthquakes are observed in non-mining areas such as the Augrabies cluster (Malephane et al., 2013), the Ceres-Tulbagh cluster (Singh et al., 2009), the Lesotho cluster (Singh et al., 2009) and unexpectedly the Leeu Gamka cluster.

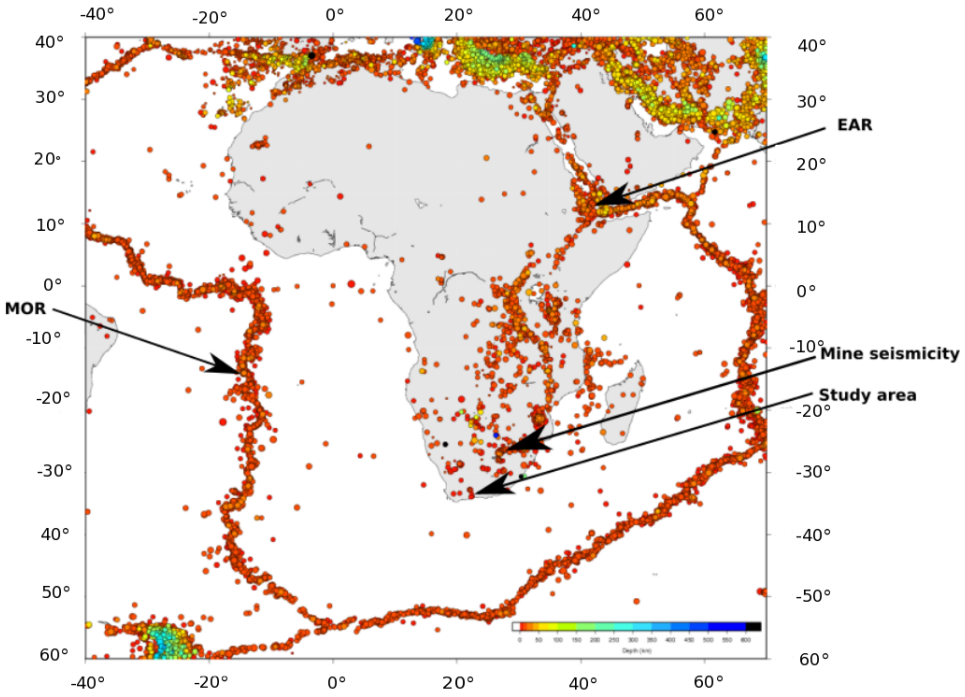

Figure 1.1: Seismicity map of Africa, based on the ISC catalogue, showing all M_L>4 earthquakes recorded between 2000 and 2017, scaled by magnitude and coloured according to depth. The image illustrates that most of the earthquakes are recorded along the plate boundaries, specifically the mid-oceanic ridge (MOR) and the East African Rift (EAR)

The International Seismological Centre (ISC) catalogue recorded 27 anomalous earthquakes in the Leeu Gamka region between 2007 and 2013 ranging in local magnitude from M_L1.7 – M_L4.5. A local array of seismometers was deployed in Leeu Gamka (Figure 1.2), covering an area of 60 km × 65 km based on the previous seismicity recorded in the region, to characterise/investigate the seismicity to determine:

- The location of the hypocentres
- The depth of the hypocentres
- The source mechanism of the earthquakes and the orientation of the structure along which the earthquakes are occurring.

This study is important because the Karoo region is currently being explored for shale

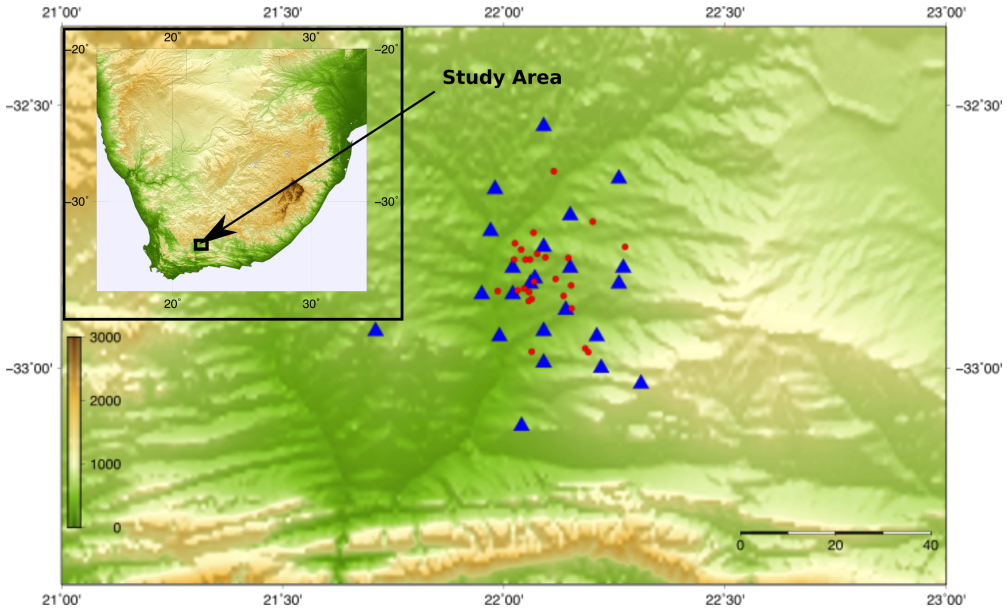

Figure 1.2: Location of anomalous seismicity recorded by the ISC between 2007 and 2013 represented by red dots and the seismic array represented by by blue triangles deployed over the Leeu Gamka region. The inset in the top left is a zoomed out version of the study area with respect to South Africa

gas to be extracted by hydraulic fracturing (De Wit, 2011; Geel et al., 2015). There is significant evidence from previous studies conducted in the United States showing that wastewater injected during the hydraulic fracturing process has resulted in a significant increase in the seismicity on faults that were not previously active and are situated close to injection wells (e.g. Davis and Pennington (1989); Horton (2012); Ellsworth (2013); Keranen et al. (2013); Frohlich et al. (2014); McGarr et al. (2015). It is therefore important to identify active faults in the Karoo and provide a baseline seismic study, prior to possible fracking activities in the area. Although the process of fracking need not involve the re-injection of wastewater into the subsurface, this method of disposal has been adopted in some regions of the United states. The pumping of wastewater, associated with the process of hydraulic fracturing, into a seismically active region can reactivate dormant faults, increase the seismicity on active faults or induce larger earthquakes than previously experienced or expected as observed in Oklahoma, also situated in an intraplate region (Keranen et al., 2013; Ellsworth, 2013). In 2014, Oklahoma recorded more earth-

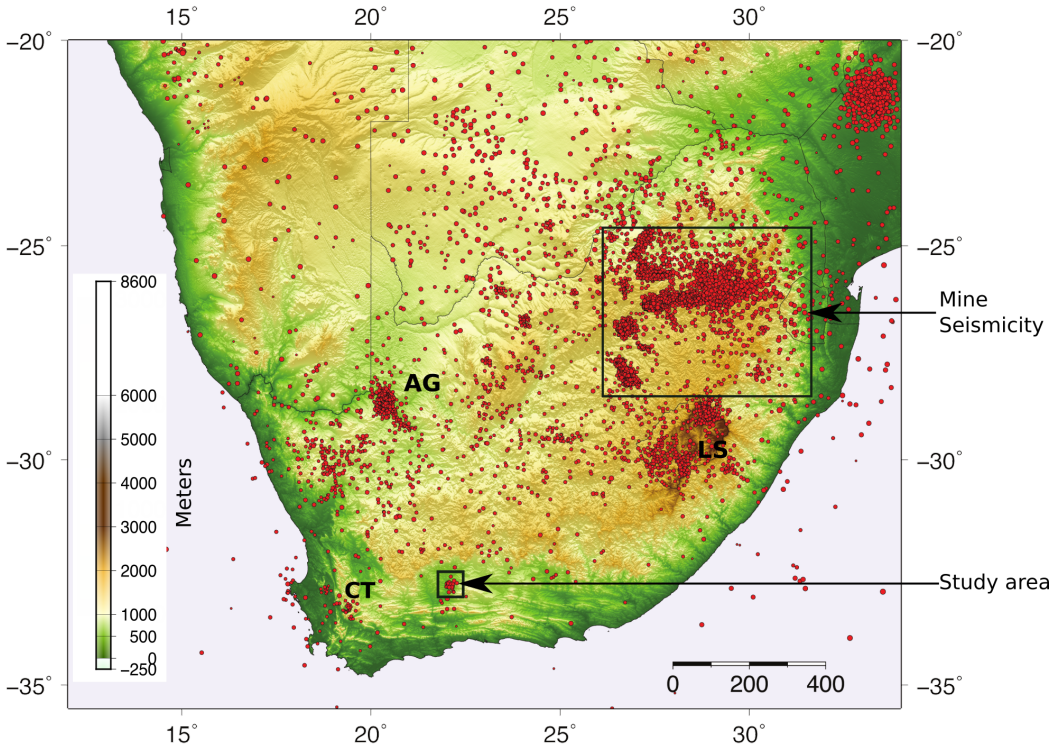

Figure 1.3: Seismicity map of South Africa. A total number of 22 089 earthquakes were recorded by the South African Network during the 20-year period between 1996 – 2016. The clusters are labelled AG (Augrabies), LS (Lesotho) and CT (Ceres-Tulbagh). The region in the small square block highlights the anomalous cluster of seismicity recorded between 2007 – 2013 in Leeu Gamka (data obtained from http://www.isc.ac.uk/iscbulletin). The mine-related seismicity is shown in the north-east region of the map.

quakes than California, which was not an artefact of an improved network (McNamara et al., 2015). An increase in seismicity due to wastewater injection can happen because the pumped fluid causes an increase in pore-pressure which reduces the effective normal stress (or clamping forces) on the fault (?Hubbert and Rubey, 1959; Raleigh et al., 1976). Constraining a structure along which earthquakes are occurring in Leeu Gamka is therefore an important outcome of this research because the pumping of wastewater close to an active fault may lead to an increase in potentially damaging seismicity.

Studies by, for example, Alabi et al. (2012) show that the southern African region is characterised by small earthquakes and that mining activities have contributed immensely to

the recorded seismicity. Figure 1.3 shows seismicity in southern Africa which is dominated by mainly induced, small earthquakes recorded near mining regions; occasionally natural earthquakes (with a tectonic source) are recorded near the Augrabies (AG) region in the Northern Cape, Lesotho (LS), the Ceres-Tulbagh (CT) region and, very unexpectedly, in the Leeu Gamka region in the Karoo.

The map of seismicity is dominated by mining regions due to two factors. Firstly, natural or tectonic earthquakes are relatively rare in South Africa due to its location far from the plate boundary zones. Secondly, seismic monitoring is concentrated around the mines due to potential risk of earthquakes to mining. This means that smaller earthquakes are recorded around the mines than elsewhere and this leads to an artificially high density of seismicity if all events are considered. For this reason, I plotted all M_{L}>4 earthquakes in southern Africa in Figure 1.4.

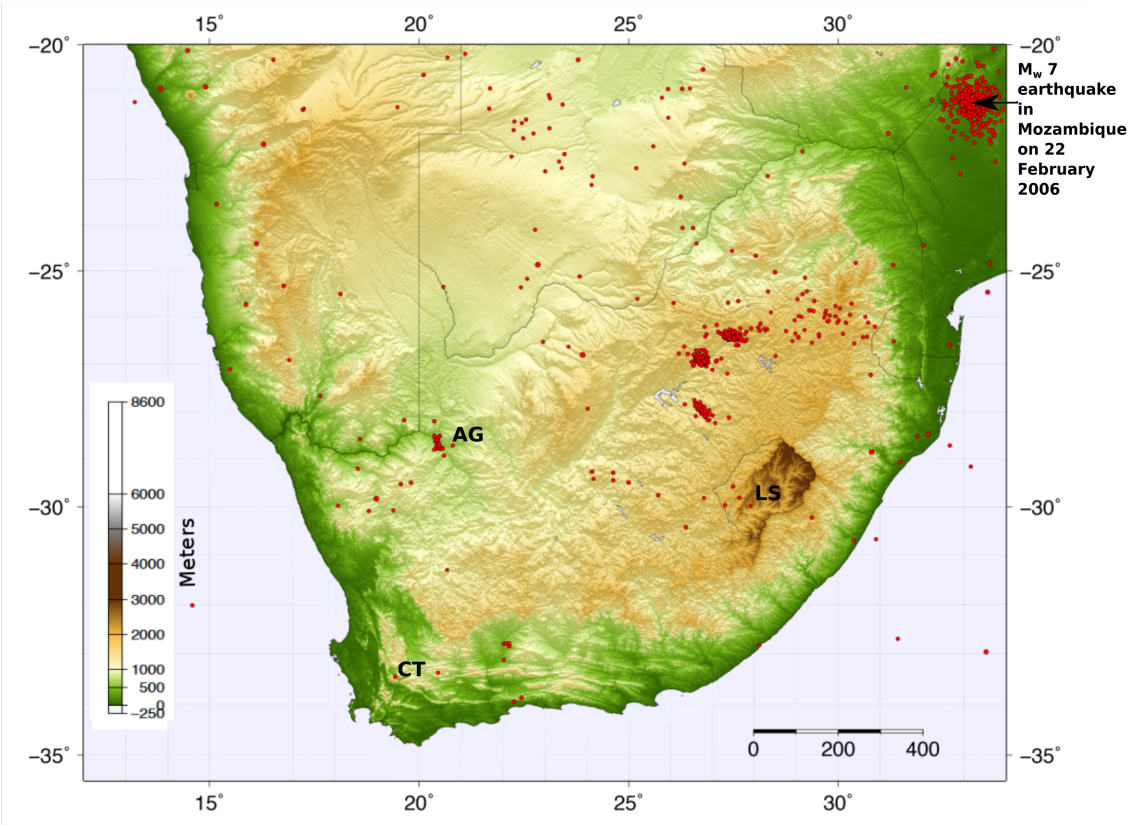

Figure 1.4: Seismicity map showing all M_{L}>4 earthquakes recorded between 1996 – 2016 in southern Africa plotted as red dots. Clusters are labelled as in Fig 1.3

The study region falls within the Western Cape province, a stable continental region (Green and Bloch, 1971; Saunders et al., 2013), the region experienced one of the largest instrumentally recorded earthquakes in South Africa, in the Ceres-Tulbagh area, CT in Figure 1.3 and Figure 1.4 (Green and Bloch, 1971; Singh et al., 2009; Smith, 2013), which resulted in nine deaths and considerable damage to property in the towns. The $M_{\mathrm{L}}6.3$, sinistral strike-slip earthquake was recorded on 29 September 1969 and the towns of Ceres and Tulbagh have continued to experience regular seismicity after the earthquake and its aftershocks (Green and Bloch, 1971; Krüger and Scherbaum, 2014) as shown in Figures 1.2 – 1.4. The largest recorded earthquake in southern Africa is located at the southern-most extent of the East African Rift System, in south-western Mozambique (Figure 1.4). The $M_{\mathrm{W}}7$ earthquake was recorded on 22 February 2006, and was unusually large considering that the earthquake was produced at a divergent plate boundary, which typically produce events with smaller magnitudes (Linzer et al., 2007). The largest mining related earthquake to be recorded in South Africa was a $M_{\mathrm{L}}5.5$ and occurred on 5 August 2014 in the KOSH mining district (Midzi et al., 2015). In the chapters to follow, I will first outline the evolution of the Karoo Basin, before summarising intraplate seismicity. I will then describe the stress controls dominant in South Africa, which influence the seismicity and the distribution and frequency of seismic events.

1.1 Geological setting

In this section, I will describe the geological setting of Leeu Gamka by outlining the geological evolution of the Karoo Basin.

The study region is situated in the Karoo Basin, approximately 700,000 km^2 in extent (Johnson et al., 2006). The Karoo sediments were deposited in the late Carboniferous (300 Ma) to middle Jurassic (180 Ma) (Johnson et al., 2006), when Pangea had reached its maximum extent (Catuneanu et al., 2005). Although the exact mechanism of basin formation remains controversial it is currently regarded by most authors as a retro-arc foreland basin developed ahead of the Cape Fold Belt (CFB) (for example Johnson et al. (2006); Catuneanu et al. (1998); Bordy et al. (2004)). Tectonic activity related to the subduction of the paleo-Pacific plate beneath the Gondwana supercontinent (Catuneanu et al., 2005; Johnson et al., 2006), was the main control on accommodation of the sediments in the basin (Johnson et al., 2006). The sediments were deposited on the stable Archean craton in the north-east and the surrounding Namaqua-Natal Belt in the south-west (Johnson et al., 2006). A contesting model proposes that the basin was formed as a result of left-lateral slip linked to the reactivation of the southern Namaqua suture, and that the boundary linked to the CFB created the late Karoo foreland basin (Tankard et al., 2012; De Wit and Ransome, 1992).

Depositional environments within the basin were influenced by the change in climatic regimes (Catuneanu et al., 2005) from glacial to aeolian as Gondwana migrated northwards from the South Pole (Johnson et al., 2006). The study area falls within the central region of the Karoo Basin which consists of the Dwyka, Ecca and Beaufort groups, a succession of glacial marine to terrestrial clastic sedimentary rocks deposited during the migration of the supercontinent from the colder latitudes at the poles to the warmer latitudes (Johnson et al., 2006). The Karoo Supergroup covers the extent of the Karoo Basin and is underlain by the Namaqua-Natal group which forms the basement rocks. The erosional contact level of the Karoo Supergroup in Leeu Gamka is at the Abrahamskraal formation in the Beaufort Group shown in Figure 1.5.

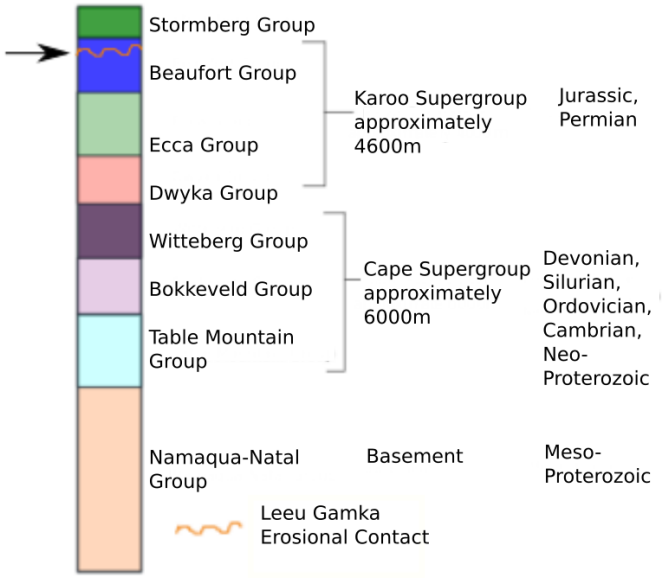

Figure 1.5: Simplified stratigraphic column of the main Karoo Basin and the arrow shows the approximate position of erosion level at Leeu Gamka; annotated thicknesses are quoted from Lindeque et al. (2007)

The Karoo Basin has always been of economic importance as it hosts all the coal deposits of the sub-continent and has recently become an attractive area for the exploration of shale gas due to its extensive size and appropriate target horizons, in particular the Whitehill formation (Geel et al., 2015). A few geophysical studies were conducted in the Karoo, including a reflection seismic survey in the Karoo by Soekor in the 1980's, a wide-angle reflection survey, a deep crustal profile over the southern Cape study and a near-vertical reflection seismic survey (Fatti, 1987; Stankiewicz et al., 2007; Lindeque et al., 2007, 2011). The studies estimated depths, thicknesses and velocities for the different lithologies and will be vital in this study for the purpose of determining an appropriate velocity model for the location of earthquake hypocentres. This information will allow for the robustness of the model to be tested.

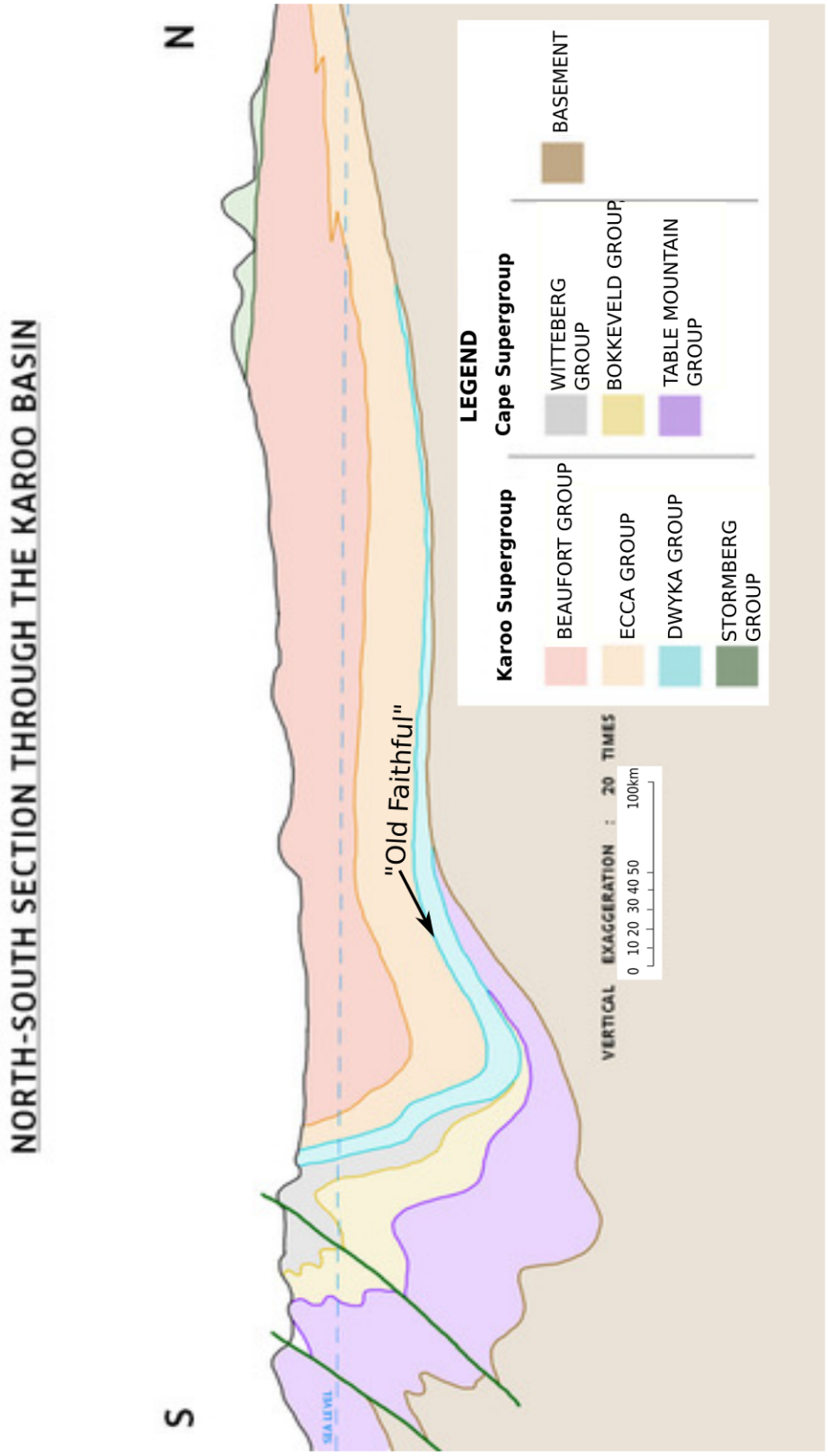

Figure 1.6: Cross-section through the Karoo and Cape Supergroup re-drawn from Fatti (1987).

One strong reflector identified in the study by Fatti (1987) was the reflector he called 'the old faithful' because it stretches over the entire Karoo basin and is thought to represent the top of the Dwyka (Figure 1.6). The second reflector identified is described as the top of the Cape Supergroup(TMS)/bottom of the Karoo Supergroup. To confirm and further support the results in Fatti (1987), Lindeque et al. (2007) provide the first clear seismic image using near vertical reflection seismics of a 100 km long crustal section of the Karoo Basin (Figure 1.7). The components of the crust they observed were the upper, middle and lower crust shown in Figure 1.7 and coloured green, orange and blue respectively.

The upper crust is relevant to the study and also confirms depths and velocities of this layer. They also confirm an unconformity between 5 km to 10 km depth, which marks the contact between the Cape Supergroup and the Karoo sediments. The Karoo basin reaches maximum depths of roughly 12 km but for the most part averages at 5.5 km – 6 km (Lindeque et al., 2011), with the TMS – Karoo boundary at 5km depth in the region of Leeu Gamka.

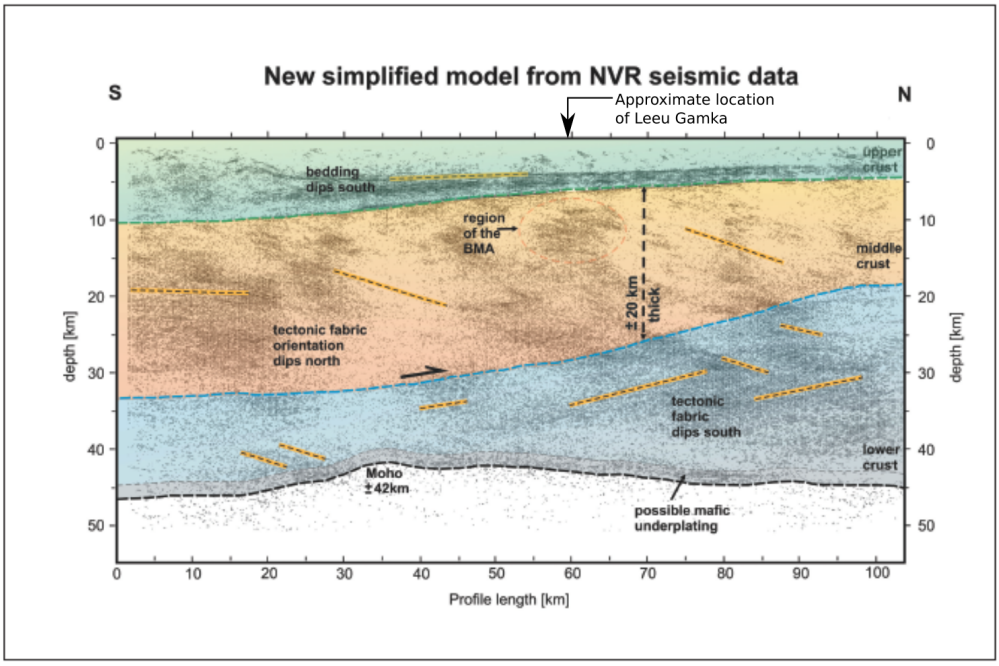

Figure 1.7: From Lindeque et al. (2011) showing a cross-section through a section of the Karoo which covers the study area (approximate location is indicated by the arrow), showing a new simplified model from the Near-vertical reflection seismic data.

1.2 Intraplate seismicity

The Karoo is located in an intraplate setting; in this section I will examine expected seismicity in such a setting. In general, seismicity is expected to be very low, but I will summarise why seismicity may occur in these regions. I will also present a few case studies of intraplate regions, from previous work around the world, and discuss their contribution to understanding this unusual class of earthquake. The link between earthquakes and wastewater injection will also be introduced in this section.

Seismic activity most commonly occurs at plate boundaries, where more than 90% of global natural seismicity occurs (Alabi et al., 2012). Large earthquakes in the interior of continents, far from plate boundaries, are rare (Calais et al., 2016) and are therefore poorly understood. Figure 1.8 shows M_L>6 earthquakes around the world. The build-up of strain which results in seismicity is less well understood in stable continental regions (e.g. the New Madrid region) where it was shown that the strain rate accumulation is at a rate which is very close to zero (Calais and Stein, 2009).

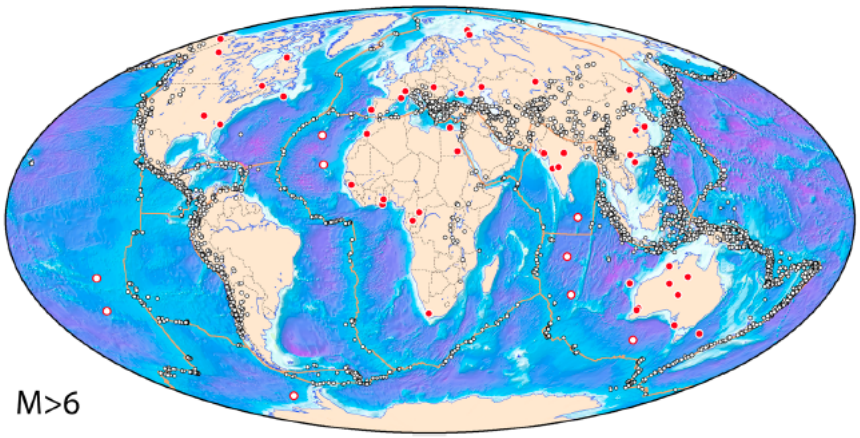

Figure 1.8: Worldwide seismic activity map showing all M_L> 6 earthquakes, red for stable continental regions, white for stable oceanic regions. Adapted from Calais et al. (2016 from http://earthquake.usgs.gov/)

Occasionally earthquakes originate in continental interiors or mid-plate regions, far from

plate boundaries (Scholz et al., 1986) and although they are rare when compared to interplate earthquakes, they can result in fatalities and significant damage to properties when they do occur. Examples include the Bhuj earthquake (India) that resulted in more than 20 000 fatalities and extensive damage (Calais et al., 2016). The New Madrid earthquakes between 1811 – 1812, in Missouri Central U.S. if repeated would be estimated to cost up to 300 billion dollars (Spencer, 2008). Even though they release only a small amount of the total seismic energy released by all the earthquakes on the planet, they tend to occur in regions where the population and infrastructure are not prepared for the consequences (Calais et al., 2016) and it is therefore important to understand the conditions in which intraplate earthquakes might occur, especially those areas whose inherent stress conditions may potentially be affected by human-induced activities.

Earthquakes located far from plate boundaries are capable of releasing large amounts of seismic energy and are often located on pre-existing structures. The potential energy that can be released on intraplate structures should not be underestimated as it has been shown that the spatial and temporal distribution of seismicity in intraplate regions can differ significantly from those at plate boundaries and can occur in regions where tectonic loading rates are close to zero (Calais et al., 2016). This makes it even more difficult to predict when a structure is loaded in an intraplate setting and sporadic earthquakes sometimes occur as a single seismic event on an old fault that has not recently been active and it seems to be a characteristic that most stable continental regions share. It is therefore important in this study, a region currently being explored for shale gas, to investigate whether a potentially active pre-existing structure can be identified, because of the seismic risk associated with the process if favourably orientated structures exist in the region. Although an area may not be very seismically active today, it could nevertheless experience a very large earthquake or more seismicity than expected. McGarr et al. (2002); Calais et al. (2016) show how intraplate earthquakes can occur in regions where previous seismicity was not recorded and no surface evidence for strain accumulation is observed e.g., the $M_{\mathrm{L}}6.3$ earthquake in Ceres-Tulbagh, South Africa 1969. This is a typical example of an intraplate region in South Africa that did not previously experience recent evidence of seismic activity and showed no evidence for strain accumulation, producing

an earthquake. The Hebron fault in western Namibia is an example of a well preserved 40km scarp with up to 10m throw that formed during a single Holocene event with no evidence for recent activity (Viola et al., 2005). The Leeu Gamka cluster of earthquakes, too, occurs in a region which shows no evidence for previous earthquake activity or a fault segment that reaches the surface; and one of the aims of this research will be to establish the possible causes for the seismicity and bring to awareness the existence of an active fault in the region.

In a study by Calais and Stein (2009), an increase in seismicity was shown to be triggered by temporal perturbations of stress in a pre-stressed crust, located near a fault that is favourably orientated relative to the regional tectonic stress field. The tectonic stress field of South Africa, as described in previous studies, will be discussed in chapter 1.3 on seismicity in South Africa. Perturbations of stress may be a result of an increase in pore-pressure at earthquake source depths, or from local changes in secondary stresses for example surface loading/unloading (Wesson and Nicholson, 1987; McGarr et al., 2002). In the Karoo these secondary stresses could originate from unloading caused by excessive borehole water extraction or in the case of possible fracking activities, the pore-pressure could be increased by waste-water injection. This can result in an increase in seismicity compared to the baseline seismicity, larger earthquakes or the earthquake sequence appearing clustered rather than persistent (Calais and Stein, 2009).

It is also possible that natural seismic swarms can be attributed to fluid overpressure (Calais et al., 2016). As well as large, infrequent intraplate earthquakes, seismic swarms can also occur in continental interiors. A seismic swarm occurs when many earthquakes in a local area are experienced in a relatively short period of time. They differ from earthquakes that are followed by a series of aftershocks in that there is no obvious mainshock in the sequence (Llenos et al., 2009). Sibson (1992), Wang and Manga (2014) and Calais et al. (2016) argue that fluid pressure at depth plays a key role in earthquakes occurring by lowering effective stress on highly stressed fault segments close to shear failure. Earthquakes can also be triggered by loading and unloading of the crust by surface or ground water. González et al. (2012) showed that changing the local stress by extracting water

from a shallow aquifer likely caused the $M_{\mathrm{L}}5.1$ earthquake near Lorca, Spain in 2011.

These studies show that the stress changes of external, non-tectonic origin can control the tectonic stress field in the lithosphere (Calais et al., 2016). This is important for an area like Leeu Gamka in the Karoo, which is currently being explored for shale gas, to be extracted by hydraulic fracturing. Earthquakes greater than $>M_{\mathrm{L}}3$ associated with fluid injection are almost always associated with the injection of large volumes of wastewater, and not necessarily the deliberate, controlled formation of fractures to liberate the gas during the fracking process (Ellsworth, 2013). The process of hydraulic fracturing which produces wastewater, which in the United States, is re-injected into the subsurface. Seismicity can be triggered by changing the pore-fluid pressure at depth. Faults usually remain locked by the pressure of an overlying column of rock and injecting fluids can counteract the pressure, making frictional failure of rocks more likely. Since the 1960s, the link between wastewater injection and seismicity has been hypothesised and experimentally demonstrated (e.g. Raleigh et al., 1976). A relationship between increased seismicity and injection of wastewater has been widely reported, for instance in Colorado, Oklahoma, Ohio, Arkansas, Texas, New Mexico and China (Horton, 2012; Brown and Frohlich; Keranen et al., 2013; Kim, 2013; Frohlich et al., 2014) and seems, as might be expected intuitively, to lead to larger magnitude earthquakes than those said to be related directly to hydraulic fracturing. This has been seen extensively in Oklahoma, also a previously seismically quiet region, where large earthquakes ($>M_{\mathrm{L}}5$) have been linked to the disposal of wastewater injection with the source locating within a few hundred meters of the wastewater injection wells (Keranen et al., 2013). Therefore, from the literature that exists at present, the evidence for a link between the volume of wastewater injection and increasing seismicity in some areas appears to be well-established and accepted. More recently, studies by Hincks et al. (2018) suggest that in addition to the volume of water injected into the subsurface, the injection depth relative to the critically stressed crystalline basement faults influences the seismic moment release.

1.3 Seismicity in South Africa

In this section I will discuss how seismicity is spatially distributed in South Africa and the main controls on the stress field. I will highlight major seismic events within South Africa and the surrounding countries and describe their seismic source. I will then describe how the stress controls influence seismicity in South Africa.

Stresses produced by relative plate motions result in frequent earthquakes at plate boundaries (Li et al., 2009). These are the most widely studied earthquakes and are relatively well-understood. By contrast, earthquakes in intraplate regions are rare and consequently lack numerous well-studied cases. Accompanying surface evidence of ruptures are generally absent (Smith, 2013) and the causes of intraplate seismicity are poorly understood. South Africa falls within this region type.

The seismicity within South Africa is dominated by mining induced earthquakes. In mining districts, earthquakes occur as a result of the sudden release of energy within a specific region undergoing deformation. Mining induced earthquakes are dependent on depth and driven by production rate and mining geometry and geological structures. Many large mining induced earthquakes occur along north-south striking normal faults and therefore accommodates east-west extension (Craig et al., 2011). There appear to be two main controls on the stress field in South Africa: The East African Rift System (EARS) and the Wegner Stress Anomaly (WSA). The extension direction observed in most earthquakes, with a normal fault source mechanism, is a function of the regional stress field which is predominantly linked to the southward propagation of the East-African Rift (Hartnady, 1990, 2002). Mining activities combined with this stress field have contributed immensely to the shallow, sporadic and scattered earthquakes recorded in the north-east regions of South Africa (Alabi et al., 2012). The East African Rift System is an active continental rift zone where the African plate is in the process of separating into two separate plates: The Nubian plate which is moving towards the west relative to the Somali plate, which is moving towards the east (Fernandes et al., 2004).

Overcoring from mining boreholes combined with focal mechanism inversion show that in general South Africa is experiencing a normal faulting stress regime with a vertical σ_1 (Delvaux and Barth, 2010) and east-west extension, which can result in strike slip faulting as is proposed for the Orkney earthquake on 5 August 2014 (Manzunzu et al., 2017). The study carried out by Manzunzu et al. (2017) after the occurrence of the Orkney earthquake analysed the aftershock sequence in order to identify the fault which might have been the source of the earthquake and an aftershock sequence. The focal mechanisms of these events were also determined using first motion polarities. The stress inversions from this study show a dominant extensional stress field in the region; and that the main earthquake had a strike-slip mechanism of faulting. This result is consistent with the dominant stress field in the region which is mainly related to the East African rift system (Manzunzu et al., 2017). The extension of the EARS system in the east of the country does also influence and produce natural seismicity and is one of the main controls of stress affecting seismicity. A second stress control has also been documented (Andreoli et al., 2009) which mainly influences seismicity in the western regions of the country; known as the Wegner Stress anomaly (WSA). Stress measurements from borehole breakouts indicate that the south-western coastal margin experiences a north-west south-eastern greatest horizontal stress.

The stress regime of the study region, Leeu Gamka, is influenced by the southern extension of the EARS (Alabi et al., 2012) and the WSA along the western coast of Southern Africa (Andreoli et al., 2009; Viola et al., 2005). These regimes are largely responsible for earthquakes of a tectonic source in South Africa and are mainly observed to the western regions of the country e.g. Ceres-Tulbagh and Augrabies.

Stress directions in southern Africa have been obtained by overcoring observations in mines (Delvaux and Barth, 2010) and stress measurements from borehole breakouts (Van Bever Donker, 1996; Viola et al., 2005). These measurements also indicate that the south-western coastal margin experiences a north-west south-eastern greatest horizontal stress. This stress direction is roughly parallel to the strike of the nodal planes observed with the Ceres-Tulbagh earthquake and Augrabies swarm (Malephane et al., 2013). Viola et al.

(2005) inferred southwest African stress evolution constrained by fracture systems and suggests a north-northwest trending greatest horizontal stress in the region.

Another factor to consider is the presence of pre-existing crustal weaknesses within which deformation is localised and possible triggered by loading/unloading/non-tectonic sources (Calais et al., 2016). There are steep shear zones in this region which are typically inherited from Pan-African orogenic belts in this part of Southern Africa (Smit et al., 2015). However, intraplate regions often lack surface features linked to an earthquake making it hard to identify active faults.

Intraplate regions deform slowly and it is difficult to identify surface geological features related to the seismic foci with any sort of precision, and therefore only a few events can be correlated to the surface geology, making them hard to study (Talwani and Gangopadhyay, 2003). The seismicity pattern study carried out by Alabi et al. (2012) established that South Africa is generally characterised by small and minor earthquakes with low spatial spread. The Gutenberg-Richter analyses estimated for the southern African region, using data from 1986 to 2009, gave the following constants a = 5.75 and b = 1.23. The frequency of earthquakes recorded from 1986 - 2017 is shown in Figure 1.9 and shows the improvements in the seismic network.

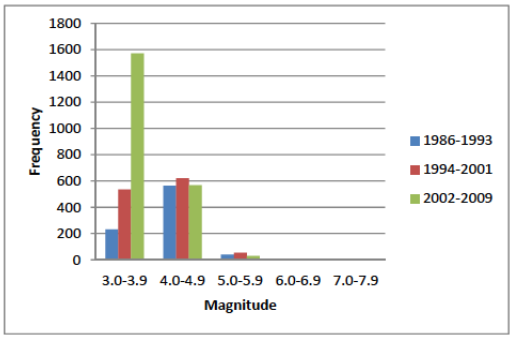

Figure 1.9: Comparison of frequency-magnitude distribution over 8-year intervals from Alabi et al, (2012), showing the number of earthquakes recorded in South Africa. The number of smaller earthquakes $M_{\mathrm{L}}3.0 - 3.9$ increased between 2002 and 2009 most likely due to the increase in the number of seismic stations and the sensitivity of the seismic network.

2 | Theoretical background to methodology

2.1 Seismology

In this section I describe the theory behind the methods applied and tools used to obtain the results in this thesis.

2.1.1 Hypocenter locations

Locating seismic events is one of the most important and oldest challenges in earthquake seismology (Shearer, 2009). Earthquakes can be located using absolute location methods or relative location methods and both methods will briefly be described in this section. Absolute location locates earthquakes relative to the stations and their positions are fixed in space; relative relocation locates earthquakes relative to each other and the locations are fixed with respect to each other. The location of an earthquake has specific information of the place and time of occurrence of energy release from a seismic event (Lomax et al., 2007). An earthquake location can be determined if we know the theoretical travel times from any source location to our receivers. We can then find the origin time for which the theoretical arrival times match observed arrival times most closely (Shearer, 2009), using a model of seismic velocities.

The process of locating an earthquake can therefore be seen as an inverse problem with four unknowns (the spatial co-ordinates of the hypocentre location and origin time). The non-linear dependence of travel times complicates the method of inverting for the best earthquake model (Shearer, 2009). The travel time in a 2-D location within a plane of uniform velocities; from a station with co-ordinates (x_i, y_i) to a point (x,y) is given by:

$$t_i = \frac{\sqrt{(x - x_i)^2 + (y - y_i)^2)^2}}{v} \tag{2.1}$$

For a homogeneous earth model, the observed arrival time t_{obs} at station location x_{obs} can be calculated as:

$$t_{obs} = t_0 + u|x_{obs} - x_0| \tag{2.2}$$

where x_0 is the location of the source occurring at the time t_0 and u is the slowness, defined as the reciprocal of the velocity ($\frac{1}{v}$). The integral is calculated over the ray path and a change in this path can be affected by changing the source location, making the equation non-linear. As a result, finding the location of a seismic event which takes the arrival times and maps them into spatial co-ordinates and an origin time, is a non-linear problem.

In this thesis I use HYPOINVERSE (Klein, 1978) to carry out an initial absolute location of the earthquakes, relative to the stations. HYPOINVERSE (Klein, 1978) uses a 1D layered model to approximate the subsurface velocity structure and solves the inverse problem using an iterative linear approach. The second method of earthquake location involves locating earthquakes, relative to each other, and the method applied in this thesis is called hypocentral double-differences, using HYPODD (Waldhauser and Ellsworth, 2000). This method was used after the initial locations had been determined to improve the locations and to remove the possible unmodelled velocity structure errors. This method uses the observed and calculated travel times between two events and the distance between the two event pairs (Waldhauser and Ellsworth, 2000). The method works best

when the ray paths from two events are nearly identical and if the events are densely distributed (compared to the average station spacing).

2.1.2 Relative relocation of earthquakes

Locating an earthquake hypocentre, using absolute location, is affected by several factors, including how the seismic array is set up, available phases, the accuracy of the picks selected, and knowledge of the velocity model of the subsurface layers (Waldhauser and Ellsworth, 2000). A one-dimensional or thee-dimensional velocity model can be used for locating earthquakes, each of these impose potential location inaccuracies due to the inhomogeneity of the subsurface layers (Waldhauser and Ellsworth, 2000). An effective way of minimising these errors is to use station corrections or relative relocation methods. The effects of errors in velocity model can also be effectively minimised by using relative relocation methods. A set of earthquakes can be located using the double-difference earthquake location method (Waldhauser and Ellsworth, 2000). The resulting locations are relative to each other. This method works best if the events are concentrated in close proximity to each other (compared to the average station spacing) and are recorded at a large number of stations (Shearer, 2009). This would the imply that the ray paths of two events to the same station would be almost identical. The method of double difference earthquake location takes the differential between the observed and expected travel-time of two events travelling to the same station (Waldhauser and Ellsworth, 2000) shown in Figure 2.1, and finds the best location for them relative to each other. This relocation method often brings structural features into sharp focus where they may previously not have been identified.

The process involves identifying and linking strong earthquake pairs (at least eight, since the number of unknowns for one pair of events is eight) based on travel-time differences observed at common stations and works by assuming that the ray paths from a source to a common station are nearly identical. Double-differences location do not require station corrections, because the unmodelled velocity is directly removed by using double differences. This is shown in Figure 2.1 where the difference in travel-time for pairs of

earthquakes of t_1 and t_2. t_1 = calculated travel-time + unknown velocity model error, t_2 = calculated travel-time + unknown velocity model + delay. When we calculate the difference between these two equations, all we are left with is the delay.

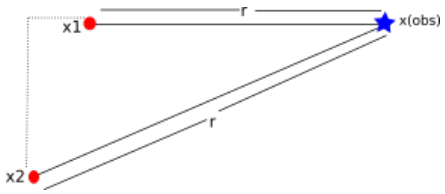

Figure 2.1: Two earthquakes, $x1$ and $x2$ and one station, x(obs) are shown to demonstrate that the travel-time delay from the event to the station, this is calculated based on the assumption that the ray paths are nearly identical.

$$\Delta t_1 - \Delta t_2 = \delta t \approx \frac{\delta r}{v} \tag{2.3}$$

where Δt is the travel time and Δt_1 - Δt_2 is the double difference.

2.1.3 Magnitude

The magnitude of an event is an important part of processing earthquake data and an important parameter of an earthquake. Historically, an empirical relation between the maximum seismographic amplitude of a given shock at various distances was established (Richter, 1935). This was done by assuming that the ratio of the maximum amplitudes of two given shocks, as registered by similar instruments at equal epicentral distances, is constant. Richter originally defined the earthquake magnitude to be proportional to the maximum recorded amplitude on a seismogram located 100 km from the epicentre. It is indicative of the amount of energy released and gives a number for the size of the event which is calibrated to the original definition by Richter (1935) which relates the amplitude to the epicentral distance. Distance is important in this calibration in that a larger earthquake will register a larger amplitude on a Wood-Anderson seismograph at a shorter distance from the source. A distance correction function would therefore need to

be applied (Gutenberg and Richter, 1944). The precision of magnitudes based on such an assumption is evidently impaired by a variety of conditions. The most obvious of these is the effect of the vertical and lateral inhomogeneity of the rock on the propagation of elastic waves at several stations, and of the instrumental constants (Richter, 1935). The most difficult of these is the first.

Local magnitude (M_{L}) can derived from the amplitude measurement on seismograms as follows (Kanamori and Anderson, 1975):

$$M_{\mathrm{L}} = \log(A) + x\log(r) + y(r) + z \tag{2.4}$$

where A is amplitude, x is geometrical spreading, r is epicentral distance, y is an attenuation correction factor and z is a base level correction factor. M_{L} is not the best magnitude scale for comparing earthquakes in different parts of the world, however, it is useful in comparing amplitudes values for local networks with relatively homogenous attenuation and geometrical spreading values and will be used in this study.

As background information it should be noted that various magnitude scales exist to communicate and compare earthquake sizes around the world. For a finite source, seismic moment, M_o is given by $\mu\overline{D}S$, where μ is the rigidity, $\overline{D}$ is the average displacement and S is the fault area. Because M_o depends on the fault state, before and after the earthquake, it does not depend on the history of faulting making it a static parameter (Kanamori and Brodsky, 2004). If M_o is determined by a seismic method, and if S is estimated by either a seismic or geodetic method, $\overline{D}$ can be determined by using the relation $\overline{D} = \frac{M_o}{\mu S}$, (Kanamori and Brodsky, 2004).

1) From seismic data: Long period waves of surface waves are least affected by propagation effects and can be used to determine M_o most accurately.

2) From geological data: A fault can be used to estimate M_o. The fault dimensions at surface may differ to the fault at dimensions at depth and the resulting estimate of M_o will

have inaccuracies. This works well for earthquakes that were not recorded instrumentally (Kanamori and Brodsky, 2004).

Seismic moments are commonly used to quantify the size of an earthquake source. Empirical, non-physical parameters were used historically to define magnitude scales. The parameters include the amplitude and the attenuation of the ray. The attenuation caused by subsurface inhomogeneity can be corrected and defining the magnitude by seismic moment, M_w, is demonstrated by the following relation (Kanamori and Brodsky, 2004):

$$M_w = \frac{log_{10}.M_o}{1.5} - 6.07 \tag{2.5}$$

M_o is a static parameter and the units used are Nm. It does not represent any dynamic properties of the source (Kanamori and Brodsky, 2004). There are, however, scaling relations that can approximate it to the total energy released at the source, at least for large earthquakes. In this sense, M_o or M_w can be used as a useful quantification parameter for an earthquake and the damage caused. In this study, however, we will be calculating the local magnitude (M_L) for the located earthquakes, which can be related to M_o, for example, by the following equation given by Thatcher and C. Hanks (1973). However the exact expression may be location dependent.

$$\log M_o = 1.5 M_\mathrm{L} + 16.0 \tag{2.6}$$

2.1.4 Magnitude-frequency distribution

Using a cumulative frequency vs magnitude plot determined from the dataset, we are able to observe the frequency of earthquakes with varying magnitudes over time, generated by a fault. This plot is commonly described by the Gutenberg-Richter relationship (Gutenberg and Richter, 1956):

$$Log_{10}N = a - bM \tag{2.7}$$

Where N is the number of earthquakes, M is the magnitude of those events, and a and b are the intercept and slope (Gutenberg and Richter, 1956). The Gutenberg-Richter relationship is effectively the ratio of small earthquakes to large earthquakes. The range of b-values are variable and depend on the spatial and temporal distribution and evolution of the seismic swarms. The higher the b-value the larger the proportion of small earthquakes to large ones.

The minimum magnitude of completeness (M_c) can be defined as the minimum magnitude above which all earthquakes in a certain region are reliably recorded (Shearer, 2009). This is usually indicated by a change in slope of the magnitude-frequency fit towards lower magnitudes. This value is crucial because a value that is too high leads to under-sampling of the data, by discarding useful data while a value that is too low can lead to erroneous seismicity parameters values and therefore a biased analysis. It is an important part of seismic hazard calculations in seismology and an erroneous M_c value can lead to incorrect b-values, which indicates the ratio of small to large earthquakes and is an indication of the seismic hazard in an area. An incorrect b-value can lead to an underestimation of overestimation of seismic hazard and also an inaccurate prediction of recurrence intervals of earthquakes of a given magnitude.

2.1.5 Focal mechanisms

Failure along existing faults will preferentially occur on suitable orientated structures (Byerlee, 1966). Earthquake focal mechanisms or fault plane solutions describe the orientation of the fault (the strike and dip) and the direction of movement within its plane (called the rake) (Kisslinger, 1980). A seismic source radiates waves which have different amplitudes and P-wave arrivals, which can either be towards or away from the hypocentre with a compressional or dilational first motion (Isacks et al., 1968). After the phases have been identified, it is possible to identify the polarity of the first motions as either being "up" or "down" and therefore compressional or dilatational. Fault plane solutions are described by two planes at right angles to each other in space, defining four quadrants which represent the first motions of the P-wave radiation pattern (Isacks et al., 1968;

Jackson, 2001). The first motions are used to determine the mechanism of failure that caused the event shown in Figure 2.2.

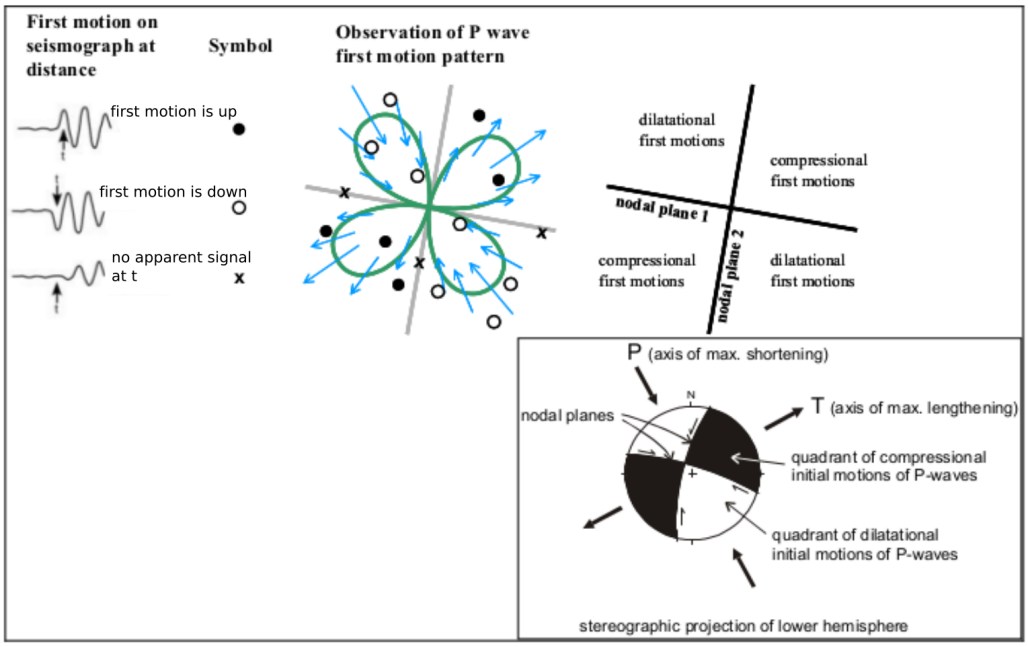

Figure 2.2: Diagram from the World Stress Map Project showing the first motion on a seismogram, the radiation pattern of the P wave, the corresponding compressional and dilatational first motions quadrants and the P and T axis of max shortening and lengthening respectively (Barth et al., 2008).

The focal mechanisms are computed to solve for the best fit to the direction of the P-first motions observed at the station. The first motion of the P-wave on a seismogram on the vertical component is used to differentiate between a compressional and dilatational first motion of the wavefront. The "up" first motion translating to compression should lie only in the quadrant containing the tension axis, and the "down" first motion of the waveform translating to dilatation should lie only in the quadrant containing the pressure axis (Kisslinger, 1980; Jackson, 2001). The mechanism of failure can be determined by the first motion polarity of P-waves on a seismogram (up or down) and these motions will differ on seismograms recorded at different stations of the same event due to the movement in either the pressure or tension axis of the focal sphere (Shearer, 2009). When the first motions of the seismograms of an event are plotted on a lower hemisphere projection

sphere, the focal mechanism of the event can be determined by observing the tension and compression (black and white areas of the spheres respectively) quadrants and are displayed on maps as beachballs as shown in Figure 2.3. The graphical representations of the faulting mechanism may also be used to make inferences about the local and regional stress regime surrounding the stations. The stress field is therefore also depicted on the beach ball. In summary the most common ways of determining the fault plane solution are described below (Shearer, 2009).

- The first motion or polarity of the P-wave arrival. By looking at the first motion of the seismic wave we can determine whether the quadrant is, either C (compression) or D (dilatational) and this information can be used for all types of earthquakes of varying distances from the source.
- Maximum amplitudes of the P and S-waves. The observed amplitudes are compared to the theoretical or expected calculated values and the best solution is found to minimise the difference.
- Moment tensor inversion. The whole or a large part of the waveform can be compared to the expected waveform and an inversion is performed for the moment tensor from which the double couple is determined.

For this study I will compute the focal mechanism by identifying the first motions of the P-wave arrival using the program FOCMEC (Snoke, 1984).

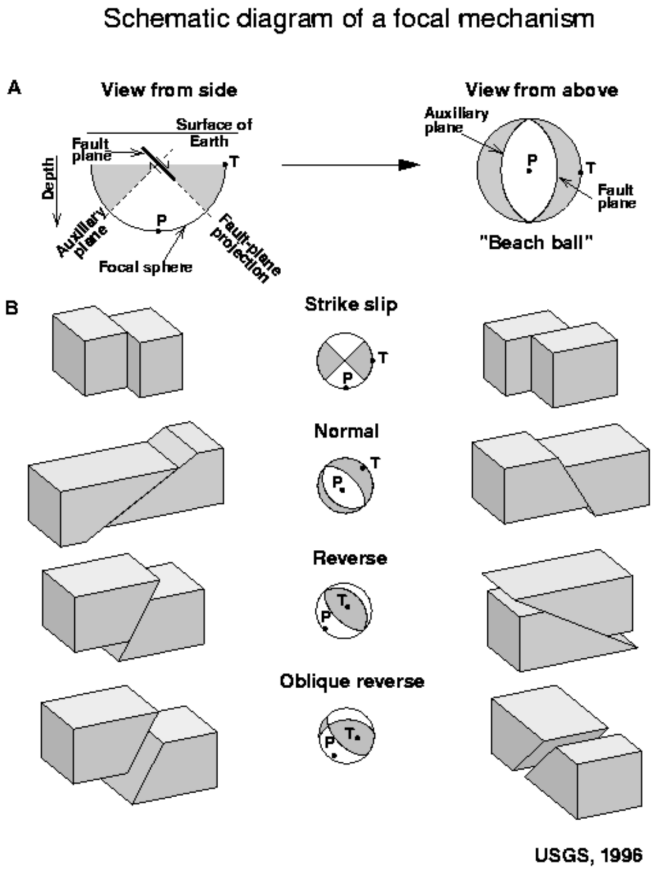

Figure 2.3: Schematic diagram of a focal mechanism showing the different modes of failure that can result in an earthquake (http://earthquake.usgs.gov).

3 | Methodology

In this section I will describe the methods used in the field and post-deployment to obtain meaningful data for interpretation. The steps taken in identifying a suitable seismic network pattern will be described. I will give a brief description of the equipment used to record the earthquakes and how the data was processed. The location methods, magnitude scale and seismic source mechanism methods will be described as well as describing and comparing waveform data and how earthquake statistics will be used.

3.1 Field deployment

The International Seismological Centre (ISC) catalogue reported localised anomalous seismicity within this region between 2007 and 2013, with local magnitudes ranging between M_{L}1.7 and 4.5. The array was centred on this zone (Figure 3.1). The apparent temporal clustering of events recorded by the ISC, however, may be a reporting artefact, because the Council for Geoscience which is responsible for submitting data to the ISC, stopped reporting data during and after this period. For this project, I deployed a temporary seismic array of 23 stations over a 65 km $\times$ 60 km centred on the anomalous seismicity. The array recorded seismicity for a period of three months. The continuous data were manually processed for P- and S-wave arrival times, hypocentral double-difference relocation, and empirically derived local magnitudes. A total of 106 local earthquakes were identified and picked from the data recorded for the duration of the deployment. The Figure 3.1 illustrates the distribution of the local network deployed for the duration of the study.

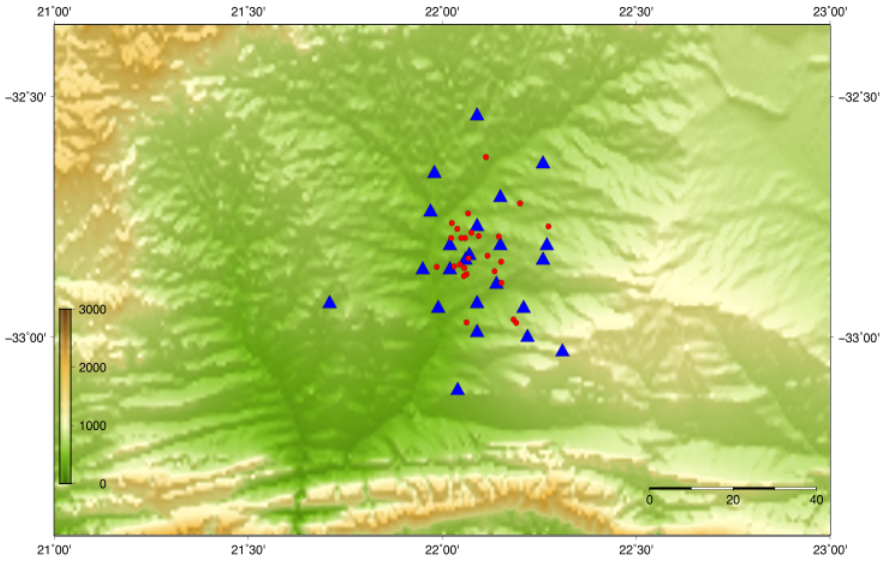

Figure 3.1: The station locations are plotted using the blue triangles centred on the zone of anomalous seismic activity reported to the ISC catalogue during the period 2007 – 2013 represented by red dots

3.1.1 Instruments

Each station consisted of a 4.5Hz triaxial geophone (PE-6/B 3-spike casing sensor) shown in Figures 3.2 and 3.3. The geophones record ground motions on the three perpendicular channels, namely, the vertical, north-south and east-west motions. Each geophone was connected to an Omnirec's DATA-cube^3 digitiser and a Pb-Zn battery to supply power, and recorded continuously at 100 samples per second for the duration of the deployment. The data were recorded with a dynamic range of 24 bits, allowing both small and large signals to be resolved. The digitisers used GPS signals for accurate timing.

3.1.2 Data Collection

The instruments were deployed on private farm land in the vicinity of Leeu Gamka, with permission from the farm owners. They were installed by digging a 30-50cm deep hole

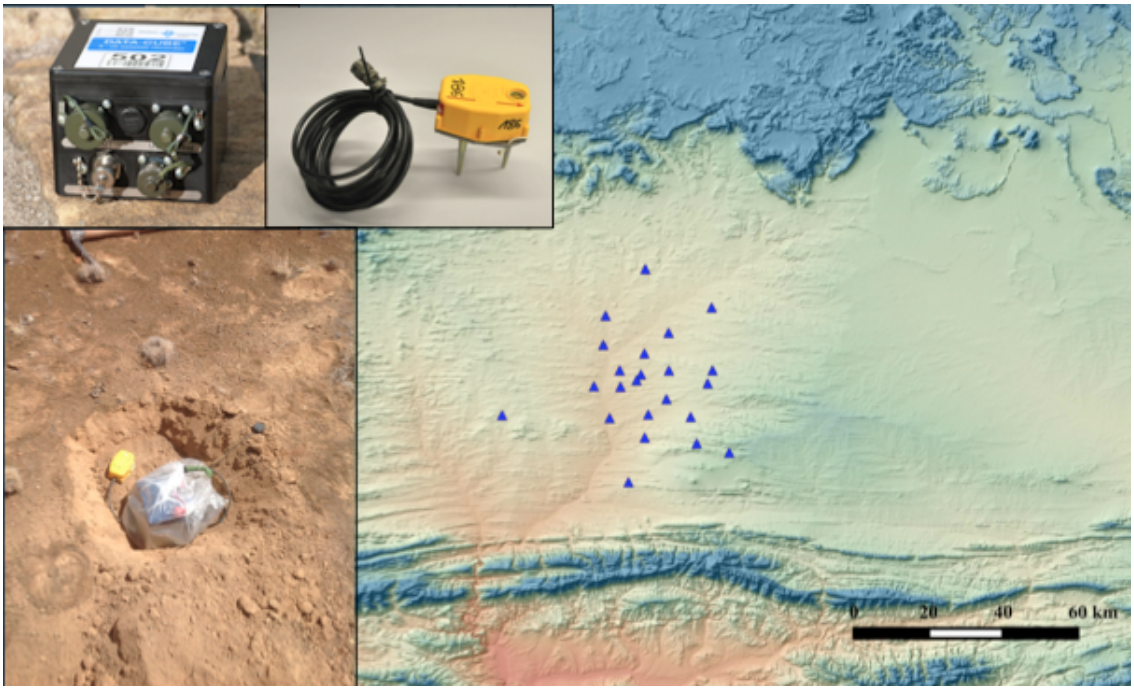

Figure 3.2: The instruments used and the distribution of seismic stations over the study area, the lower photograph shows the equipment in the ground in water-tight bags.

Figure 3.3: 3-channel Omnirec's-cube^3 digitiser connected to a triaxial 4.5Hz geophone. A Pb-Zn battery and an external GPS antenna exposed to the sky to ensure good satellite detection.

(shown in Figure 3.2) as far away from main roads and farm activity as possible, in sand or broken shale bedrock, in order to minimise the amount of ambient noise recorded. The north arrow on the instrument was aligned to true north. The geophone was placed in the hole; the spikes of the instruments allow for good coupling with the ground; the spirit-level ensures horizontal positioning of the instrument. The data cube along with the external battery was placed in a durable plastic bag and sealed with waterproof tape. The hole was then back-filled leaving only the GPS antenna exposed to the sky to ensure good GPS connection. A rock marker was placed next to the antenna to aid with location of the station during collection. After three months the instruments were collected from the field. All the instruments were recovered with no damage except for one instrument, where the GPS antenna had been ripped off by either an animal or human. Most of the instruments were still recording at the time of collection although some had just run out of power; I had anticipated that the batteries would last for 3 months.

3.2 Data processing

The program SEISAN (Havskov and Ottemöller, 1999) was used for the interpretation of seismic data collected during the deployment period. A few short scripts were written in order to convert the digital data into a compatible format for use in SEISAN (Havskov and Ottemöller, 1999) and to trigger events by using a selected frequency range. Once this procedure was performed, the events were written out into the DAT file in SEISAN to be ready for processing. The first step in the procedure was to identify local and regional events based on the waveform. The difference is clearly identifiable by the arrival time difference between the P- and the S-wave, in a regional event the time taken for the arrival of the S-wave after the P-wave is much longer than in a local event. The amplitude of the P-wave is much smaller in a regional event and the surface waves are recorded for longer, where as in the local events, the P- and S-waves are generally easy to identify, with shorter durations recorded for the S-wave. The seismograms of various stations triggered by a local seismic event is shown in Figure 3.4.

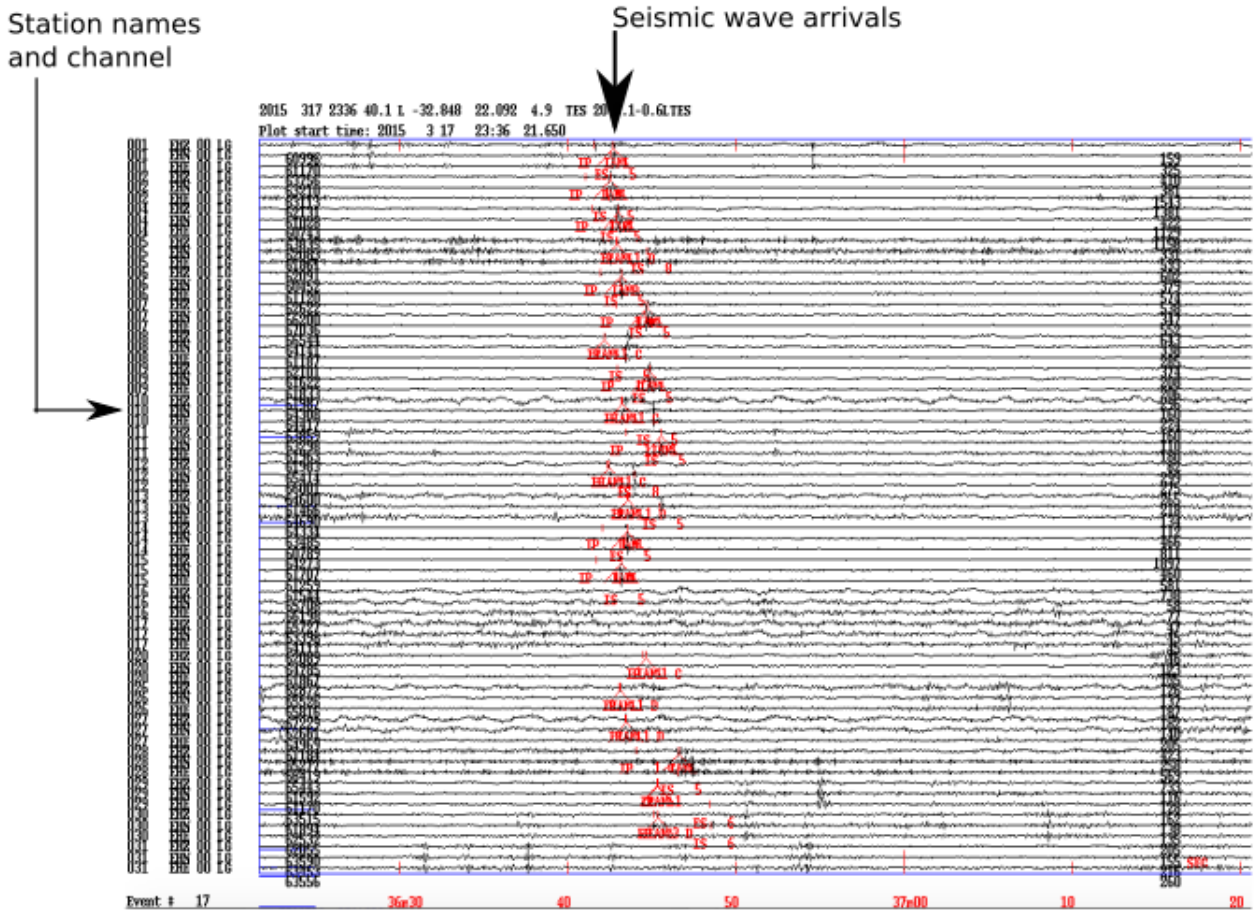

Figure 3.4: The seismograms of various stations triggered by a local seismic event, showing all three channels for each station and the arrivals of the P- and S-waves.

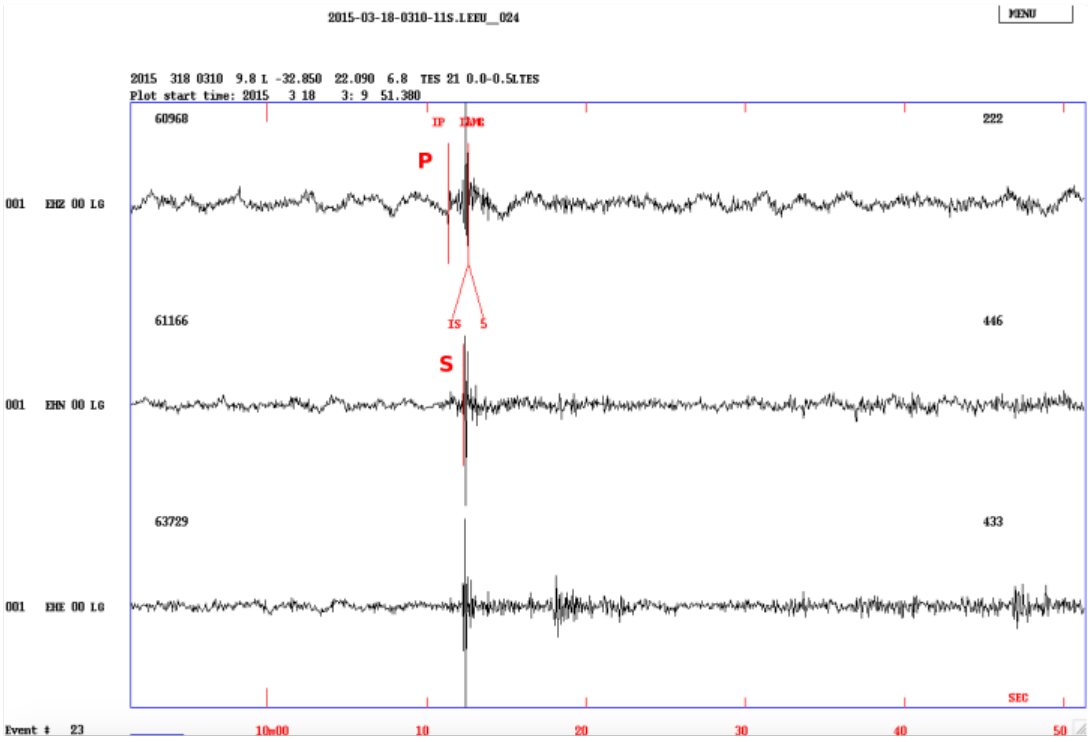

Figure 3.5: The seismogram of one station with the amplitude changes on all three channels and the arrival of the P- and S-waves

The next process in the procedure is to pick arrivals of the P- and S-waves, using the cursor, from 3-component stations surrounding the event. Once the event is selected the waveforms of the triggered stations will appear showing the waveforms recorded on all three components, E, N and Z. The process is called "phase picking". Each channel can be singled out and various filters and zoom options applied in order to make accurate picks of the arrival times as shown in Figure 3.5).

The arrival of the first wave recorded at the station is the P-wave and can be observed by a marked visual change in the amplitude or frequency or both as shown in Figure 3.6.

The P-wave is recorded more strongly on the Z channel, because the ground motion is parallel the direction of wave propagation (up, down) or the arrival of the incident P-wave from the source. Complexities can arise in identifying this wave arrival when the

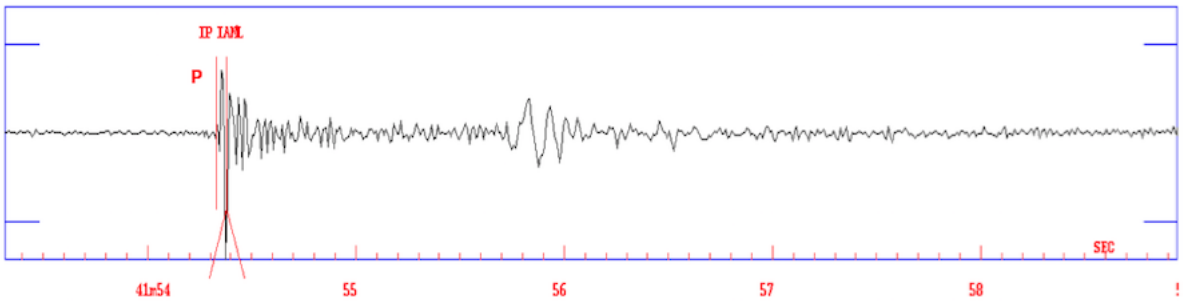

Figure 3.6: Seismogram showing the arrival of the P-wave on the vertical channel.

waves are superimposed by P-wave coda or when we have a low signal to noise ratio. The picks can be weighted according to the confidence of the arrival and the clarity of the waveform. A confidence can be assigned to the pick, where a confidence level of 1 represents maximum certainty, decreasing in confidence to 4.

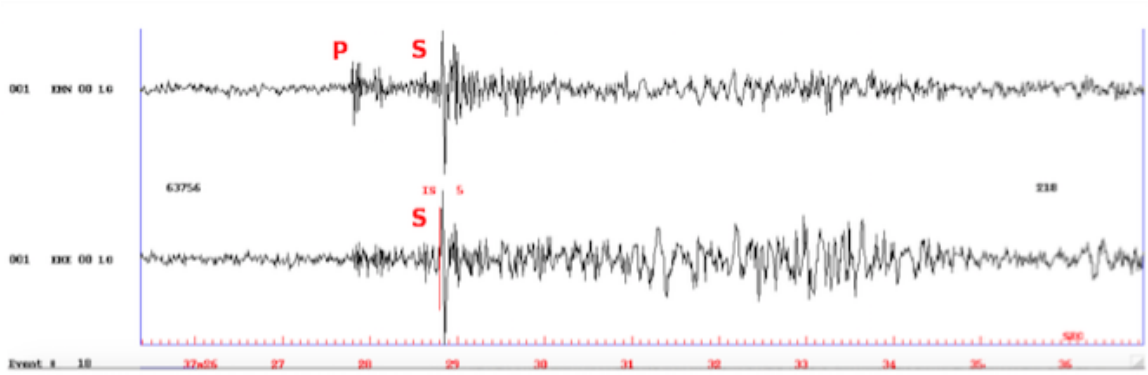

Figure 3.7: Seismogram showing the arrival of the S-wave on both horizontal channels.

The S-wave causes particle motion perpendicular to the direction of the wave. Since the angle of incidence of the S-wave is near vertical at the station, and the S-wave causes particle motion perpendicular to the direction of the wave arrival, the S-wave arrival will be recorded most strongly on the horizontal components shown in Figure 3.7 and 3.8.

The seismograms recorded the ground motion as a result of the energy released during an earthquake but also recorded background/ambient noise which is generated by man-made activities such as farming, windmills, traffic or heavy machinery and natural noise from

wind, atmospheric phenomena and ocean waves. The waves produced by different sources will have different wave properties, which are important to identify when picking phases. We can zoom in and out of the wave form in order to accurately pick the arrival of the P- and S-waves. In instances where the waveform is superimposed with P-wave coda or background noise, the software has a bandpass filtering function that allows frequencies between a low and high cut-off limit to be viewed while blocking frequencies not in this range. Ideally low frequency noise should be filtered out which included teleseismic earthquakes and trucks and machinery as well as the high frequency data which includes noise from wind, atmosphere, oceans, windmills, cars and other anthropogenic sources, in this case we may need to filter the waveform to get rid of this noise and improve the signal-to-noise ratio, when picking phases.

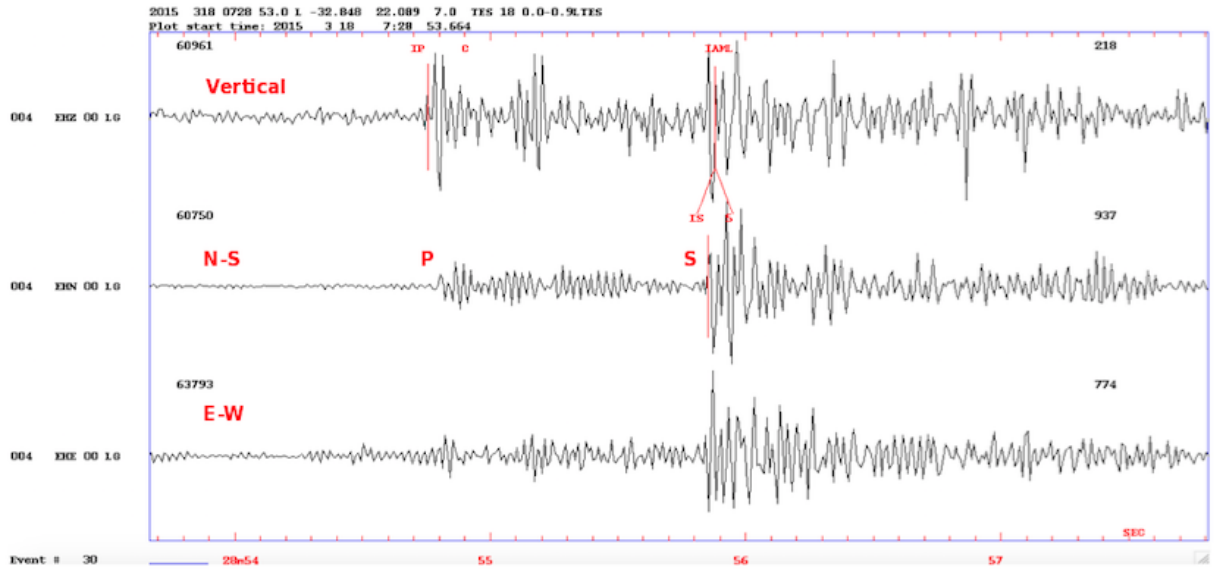

Figure 3.8: Seismogram of one station showing the zoomed in waveforms with P- and S-waves picked on all the channels.

3.2.1 Filtering

A band-pass filter was applied to stations which were noisy and difficult to analyse. The filter improves the signal-to-noise ratio, with a minimum low and maximum high

cutoff filter of 15 Hz and 25 Hz, respectively. Improving the signal-to-noise ratio makes identifying amplitude differences, particularly at the onset of a P- or S- arrival, easier to identify. However, adding a filter changes the waveform and the filter must therefore be removed before choosing the final P- or S- pick. Filtering the data will improve the signal to noise ratio, making the arrival of the P- and S-waves more clearly defined, but should only be used as a guide in identifying the arrival time. The actual selection of the pick should be done on the unfiltered data. An example of unfiltered data on the vertical channel is shown in Figure 3.9.

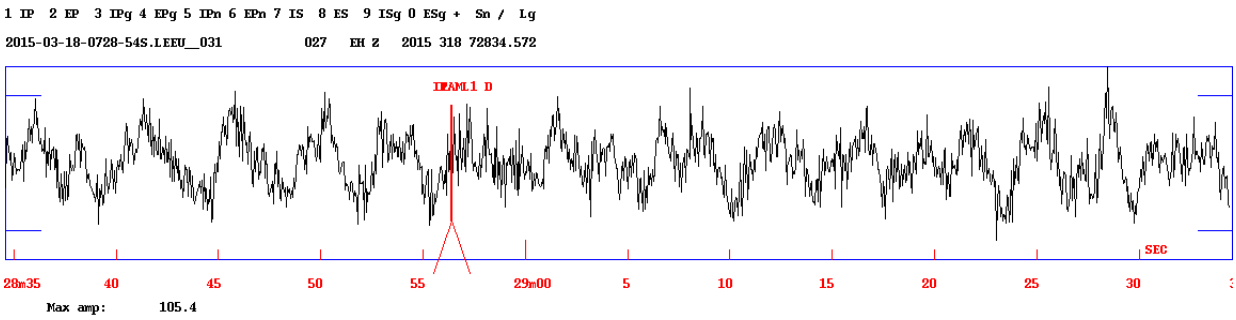

Figure 3.9: Unfiltered data from the z-component of a seismogram recorded on 18 March 2015 at 07:28 showing the hidden high frequency P-arrival marked by the red line.

Arrival times are weighted according to the accuracy of the picks and this is taken into consideration when the calculation of the hypocentres is carried out. As mentioned in the previous section, the pick can be weighted from 1 - 4, where one is the allocated to a waveform with high confidence of the pick and 4 is allocated to a pick with low confidence. A weight of 1 is assigned to a clearly identifiable pick with no background noise with no ambiguity. In instances where the waveform needed to be filtered a weighting of 2 or 3 was given. In instances where the waveform is superimposed with background noise and even filtering cannot reveal the arrival time time, but the relative position of the pick is known, a weight of 4 was used. An example of filtered data on the vertical channel is shown in Figure 3.10.

Synthetic picks can be generated, which are determined from the velocity model and the expected arrival times of the P- and S- waves at a particular station as shown in Figure

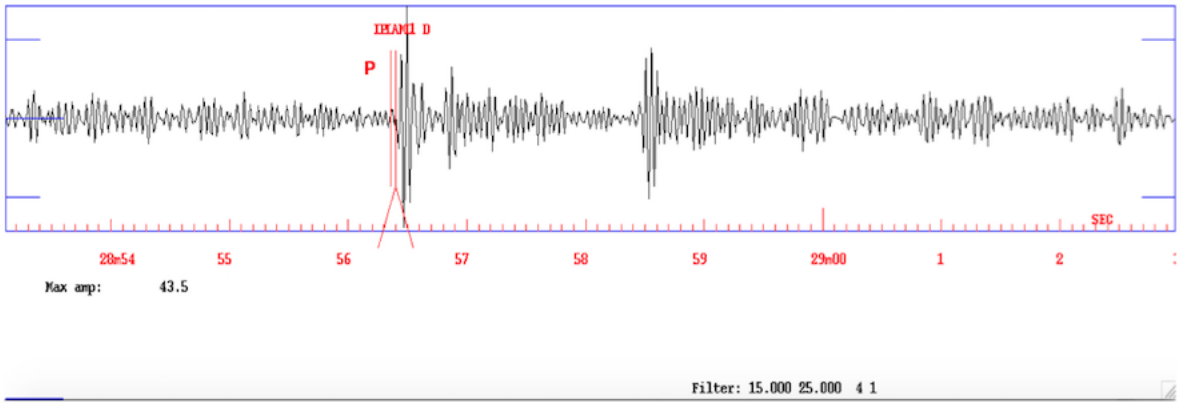

Figure 3.10: Filtered data with a bandpass of 15 - 25Hz, which increases the signal-to-noise ratio and emphasises the P- and S-waves

3.11. This can be used, with caution and as a guide, to help identify the expected arrival of a wave if any ambiguity exists when the P-wave coda or when the background noise makes identifying the arrivals, difficult. It should not be used to select P- and S-wave arrivals, as this will introduce errors in the location of the earthquakes.

The errors or residuals are an indication of the difference between the observed and expected arrival times of the P- and S-waves. Ideally, this residual value should be minimised by the synthetic pick being as close to the actual pick as possible, in order to increase the confidence of the picks. When a significant picking error has been made however, the residual value on all the stations will be affected and the synthetics will therefore not be a good guide on the expected arrivals. The residual value should be as close to zero as possible. The greater the number of picks for each station, the more reliable and stable the location of the hypocentre will be. The more S-picks we have, the more robust the depth component of the calculation. The waveforms recorded in this study are very high quality with good signal-to-noise ratio, therefore the velocity model can be improved by adjusting the V_p and V_s ratio to get the lowest residual value. Adjusting the thickness of the layers in the velocity model will change the epicentre depths and therefore the aim of this study is to determine the sensitivity of the locations (in terms of depth) to the thickness and velocity of the various layers.

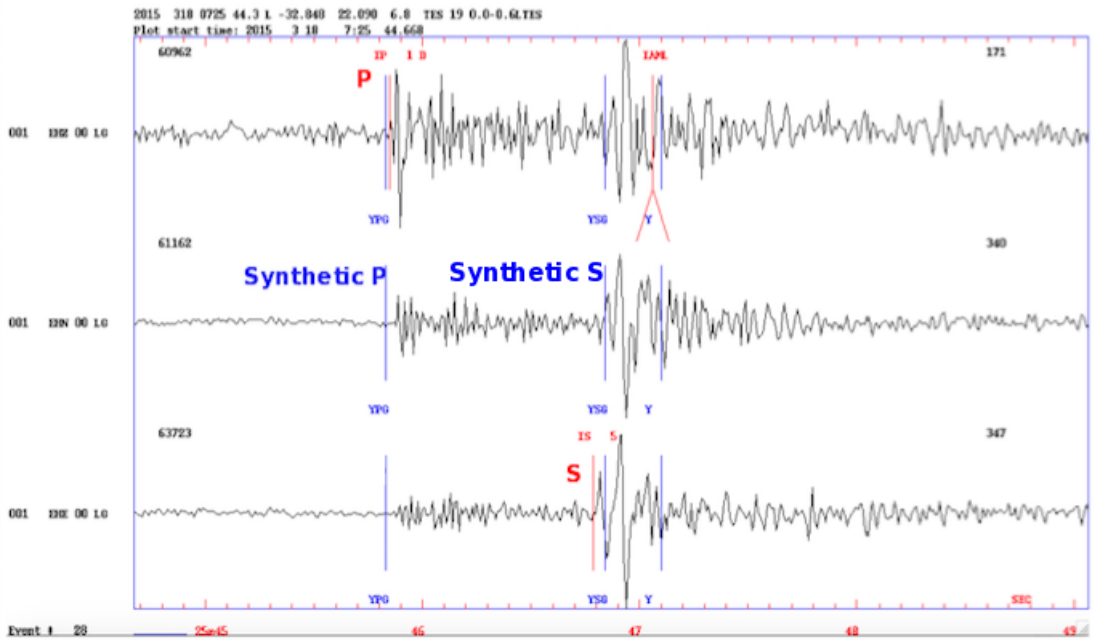

Figure 3.11: The synthetic picks vs the actual picks of both the P-wave and the S-wave.

3.2.2 Locating events

Locating the seismic events was performed once all visible P- and S-wave arrival times had been picked on all stations for a particular event. Synthetic picks are produced by HYPOINVERSE (Klein, 1978) in SEISAN (Havskov and Ottemöller, 1999) using a selected velocity model. Once a location is performed an RMS value is calculated by determining the root-mean square distances (minimised) between the synthetic picks and the selected picks (i.e. the calculated and the observed travel times). When the data is noisy or there is a low signal-to-noise ratio the initial pick maybe incorrectly selected. This will be confirmed by a very large error in the RMS value and the synthetic picks can therefore be used as a guide. A file is produced that can be used to plot the hypocentres in Google Earth.

3.2.3 Velocity model

The accuracy of the velocity model used for calculating hypocentres is important in determining the location of the earthquakes, and naturally, an inaccurate model will result in inaccuracies in the location. Using Karoo and Cape Supergroup thicknesses and velocities from the literature (Fatti, 1987; Lindeque et al., 2007; Stankiewicz et al., 2008; Scheiber-Enslin, 2016) available for the region, a suitable velocity model was derived, because using the standard Crust1.0 model was not appropriate for this region. Two distinct reflections were established in the literature, which are applicable to the model. The depth to the top of the Dwyka ("old faithful ") and the depth to the base of the Karoo (approximately 4 km and 5 km respectively). These two distinct reflections are a consequence of acoustic impedance differences between the lithologies and were used in the model.

For this study, the base of the Karoo is assumed to be at a depth of 5 km and the top of the Dwyka, another strong reflector observed from the literature is assumed to be 1 km above the base of the Karoo. The velocities used for the top layer to the top of the Dwyka is 5.5 km/s and the layer to the base of the Karoo is assumed to be 6 km/s (Fatti, 1987). The weaker reflectors are the Witteberg-Bokkeveld group contact and the top of the Table Mountain Group of the Cape Supergroup are not considered in the model. The Crust1.0 model for thicknesses and velocities were used for the rest of the layers below the Karoo Supergroup because they would be more or less the same as the faster TMS and Basement rocks. The ray paths would not be heavily influenced by the deeper lithologies. Previous work by Midzi et al. (2010); Saunders et al. (2016) suggest and show how choosing an appropriate velocity model and adapting it for different tectonic regions for the SANSN network, helped to improve location accuracies.

An important outcome of this research was to establish whether the earthquakes recorded plot within the Karoo, or in the Cape Supergroup. It is for this reason that the top two

reflectors were used in the model, as they will have slower velocities than those in the top layers of the Crust1.0 model and the deeper lithologies. I did not, however, invert for a velocity model for this thesis. A velocity-hypocentre inversion is performed to invert the observed travel-times of seismic waves for all events in the database simultaneously, which calculates the possible ray paths of seismic waves based on the observed travel-times for hypocentre locations while simultaneously solving for phase velocity within pre-determined layers below the array. When we have many widely distributed earthquakes in a region, this method of inversion works well because the velocities will not be homogeneous across large distances. However, if the events are extremely localised, as will be shown in the results section, for this study it is more difficult to invert for a robust velocity model. In this case I took the CRUST1.0 model (http://igppweb.ucsd.edu/ gabi/rem.html) and modified it to include upper crust velocities and thicknesses that are relevant to this study, as opposed to a global model and kept the deeper velocities and thicknesses the same as the global model. The unique model chosen for this study is shown in Table 3.1.

	Depth (km)	Vp Velocity (km/s)	Vs Velocity (km/s)
Sea level	-1	5.00	3.13
Top of the Dwyka	2	5.50	3.44
Base of the Karoo	4	6.00	3.75
	17.15	6.70	4.19
	32.92	7.00	4.38
MOHO	48.69	8.16	5.10
	60	8.20	5.13

Table 3.1: The depth to the layers in the velocity model as well as the V_p and V_s values used for locating earthquakes in SEISAN is shown in the table.

Each of the layers have explicit V_p values as well as depths to the layer, shown in Table 3.2, that can be varied in the model. The model allows for a V_p/V_s ratio to be selected, as opposed to selecting explicit V_s values for each layer. The V_p values selected for the layers to the top of the Dwyka and the Base of the Karoo were based on values from the literature (Fatti, 1987; Lindeque et al., 2007; Stankiewicz et al., 2008; Scheiber-Enslin, 2016) and an appropriate V_p/V_s ratio was selected by ensuring that the RMS average for

the earthquakes were reasonably low (closer to zero). The V_p/V_s ratio resulting in the lowest RMS value was selected for the model.

	Vp/Vs 1.6	Vp/Vs 1.7
Top of Dwyka 3km Base of Karoo 5km	0.069	0.076
Top of Dwyka 10km Base of Karoo 12km	0.080	0.092

Table 3.2: The RMS values obtained when varying the V_s and V_s values are shown in the table. A higher V_p/V_s ratio of 1.7 as well as unreasonable depths to the Karoo layers results in higher RMS values

3.2.4 Magnitude-frequency distribution

Using a cumulative frequency vs magnitude plot determined from the dataset, we are able to observe the frequency of earthquakes with varying magnitudes over time, generated by a fault. This plot is commonly described by the Gutenberg-Richter relationship (Gutenberg and Richter, 1956):

$$Log_{10}N = a - bM \tag{3.1}$$

Where N is the number of earthquakes, M is the magnitude of those events, and a and b are the intercept and slope (Gutenberg and Richter, 1956). The Gutenberg-Richter relationship a measure of the relative occurrence of small to large earthquakes. The range of b-values can vary widely and depends on the nature and spatio-temporal evolution of earthquakes swarms. The higher the b-value the larger the proportion of small earthquakes to large ones.

The minimum magnitude of completeness (M_c) can be defined as the minimum magnitude above which, all earthquakes in a certain region are reliably recorded (Shearer, 2009). This

is usually indicated by a change in slope of the magnitude-frequency fit towards lower magnitudes.

3.2.5 Focal mechanisms

One of the aims of this thesis was to produce focal mechanisms for the larger events which were recorded on more than 18 stations. The more stations which record the event the more confidence we have in defining the compressional and tensional axis. The direction of first motion was picked on the seismograms, i.e the polarity of the P-wave on the trace (up or down on the vertical component) along with the P- and S-wave picks. The individual fault plane solutions have very similar nodal planes and assuming that events recorded (with the highest triggers) within a similar stress field will generate similar solutions, we can group the solutions to make one fault plane which will represent an average solution.

When selecting the P-wave arrival in the picking phase, the polarity of the P-wave trace was also selected i.e. up or down on the vertical component, and saved along with the picks for potential use in focal mechanism derivation. The program used to perform this derivation is FOCMEC, also a component of the SEISAN software. Conventionally we represent the compression and dilatational regions as black and white, respectively. Hence we can represent the faulting and focal source mechanism with a beach ball plot (refer to Figure 2.2).

The composite moment tensor was calculated for this study by a joint inversion of several earthquakes recorded from the same fault system, displaying similar waveforms and focal mechanisms. (Vavryčuk, 2015). The method analyses the full waveform and uses the amplitudes of the P and/or S waves or full waveforms. Because the inversion is linear, it is most useful for large earthquake datasets. The method is particularly useful in the analysis of microseismicity, earthquakes swarms, or aftershock sequences, where observations of multiple earthquakes in a localised area are available.

The conditions that should be satisfied in the composite moment tensor inversion include the following (Vavryčuk, 2015):

1. Sensors should ensure good coverage of the focal sphere
2. Amplitudes or waveforms of events have good signal-to-noise ratio
3. The velocity model is well known, and
4. Event locations are accurate.

In addition, a dataset of at least several events with similar focal mechanism is required, and the events should have different locations in order to be stable.

3.2.6 HYPODD relocation process and varying the parameters

Where possible, the earthquakes were relocated in order to minimise the RMS value calculated in the original location of the hypocentres, using relative relocation. The program HYPODD (Waldhauser and Ellsworth, 2000) was used to identify good earthquake pairs based on selected parameters. When the events are relocated with this method it often sharpens structural features which could not be previously identified. A least-squares solution is found by iteratively adjusting the predicted and observed differential times between foci pairs. The double-difference method minimises errors due to unmodelled velocity structure without the use of station corrections. The method improves the precision of the relative hypocentre locations, transforming data from a cloud or cluster of earthquake locations into a sharpened image, allowing the identification of structures such as fault planes. See more detail about this method in section 2.1.2 describing the HYPODD relocation process.

The method has been shown by several studies to be amongst the most accurate of the relocation methods. The location accuracy, however, strongly depends on the parameters used in the input files. If the control parameters are chosen well, the location errors

can be significantly reduced. Bouchaala et al. (2013) showed that no distortions such as artificial clustering of hypocentre locations, as observed in this study in the initial locations of the Leeu Gamka earthquakes, is introduced if relative relocations are used. This method helps reveal detailed geometry of active fault zones or structures.

The classic absolute methods for locations of earthquake hypocentres are based on calculating the differential between the travel-time of two events from the same station eliminating the inaccuracies in the velocity model. The accuracy of these methods is controlled by errors in the picking of the first arrivals of the P- and S- waves. The errors introduced by the structural inhomogeneities in the subsurface layers can be significantly minimised using the relative relocation methods. The double-difference method effectively lowers the error between the predicted and observed differential times between pairs of earthquakes (Waldhauser and Ellsworth, 2000).

The double-differenced locations can be calculated using the HYPODD method designed and published by Waldhauser (2001). The location approach in this method is controlled by several parameters. One of the approaches include the distance between the event hypocentres forming a pair. This parameter will identify the size of the cluster and also the number of clusters used for relocation. In addition, it controls the number of events used for the relocation from the original dataset. The maximum number of neighbouring events is limited by the maximum neighbours parameter. Bouchaala et al. (2013) tested the sensitivity of the various parameters and found that the most accurate locations, when varying the maximum separation parameter between 20 to 1km, are found for a value of 1km. A high value selected for the separation distance allows for a large number of earthquake pairs to be used for relocation (Bouchaala et al., 2013).

The maximum number of foci pairs are controlled by the maximum neighbours parameter. When the maximum neighbours parameter is set to 3 km, for example, this means that a maximum of three foci pairs is possible for one event. Increasing the total number of foci pairs in the input file decreases the location error (Bouchaala et al., 2013).

Thirdly, the dependence of the number of stations was tested to check the effect location

precision. The maximum number of observations controls the number of stations used in the calculation. As expected, the error is inversely proportional to the number of stations. One should ideally use the number of stations in the seismic array for this parameter. Only strong neighbours are considered for relocation and the events included will be determined by the minimum link parameter which will select the minimum number of linked neighbours. The hypocentral separation selected between two earthquakes should be small compared to the event-station distance.

3.2.7 Waveform Comparisons

The earthquakes recorded during this study plot in close proximity to each other and will, assuming a similar focal mechanism, therefore have similar waveforms and similar event-station raypaths between events. It was for this reason the the hypo-double differencing technique was applied and we expect that if the wave travels a similar raypath from event to station, that the waveforms will look similar. The waveforms of closely located events were assessed and their similarities compared.

Similar waveforms are produced when earthquakes share the same mode of failure and are co-located (i.e. share the same ray paths between source and receiver). When the hypocentres are co-located within the location errors and the estimated source errors overlap such that it is assumed that the same section of the fault is rupturing each time. Although 106 earthquakes were recorded, they essentially locate in the same area.

3.2.8 Earthquake statistics

Statistical analysis methods were performed on the data. The activity rate over the three-month period was assessed in order to assess the temporal distribution of the earthquakes for the duration of the deployment. The depths calculated from SEISAN are plotted against longitude in order establish if a trend in the overall data set, with respect to the position of the located event, is evident. A histogram was plotted to show the distribution

of calculated magnitudes over time in order to estimate the magnitude of completeness. The b-value value was determined from the Gutenberg-Richter plot using the maximum likelihood method (Aki, 1967). The confidence of this value can be determined using the Shi and Bolts equation (1982) of probability which estimates the interval of a b-value at a certain confidence level.

4 Results

The results obtained will be shown and described in this section followed by an interpretation of the data in the chapter following this one. The earthquake depths, spatial and temporal distribution will be discussed and how the velocity model selected for data analysis can influence the results. The source mechanism and stress conditions will be described followed by a section concluding the study.

4.1 Time-History distribution

The seismic events were recorded during the period between 6 March 2015 and 28 May 2015 and occur sporadically as shown in Figure 4.1. The initial locations of the events are found in the same region as the events identified from the 2007 – 2013 cluster of events recorded by the National Seismic Network. The cluster has a general NW – SE orientation and generally shallow seismicity ranging between 1 km and 12 km depth, with a concentration of earthquakes between 6 km - 7 km depth. The spatial distribution of the microseismic events recorded during the deployment period are shown in Figure 4.2.

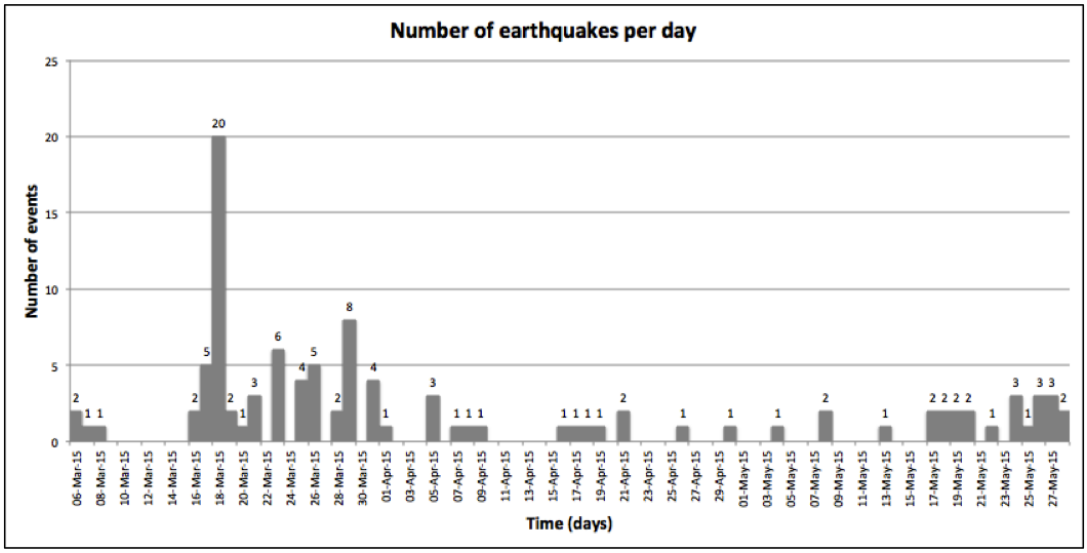

Figure 4.1: Showing the distribution of the seismic events throughout the deployment period. Each solid grey bar represents the number of earthquakes recorded per day.

In Figure 4.1, the number of events per day are represented by the grey bars. This time-history plot of the seismicity recorded over the three month period, shows that the seismic sequence experienced periods of high activity alternating with periods of seismic quiescence. The events are sporadically distributed with four events recorded on the first three days followed by inactivity for seven days. The activity revived with the highest number of events recorded between 16 March and 1 April 2015. This surge of events represents 60% of the total number of events recorded (64 of a total of 106) during the deployment. This cluster of events is not preceded by a large event nor does a large event follow this sequence. The activity is scattered over time between 2 May and 16 May 2016.

4.2 Hypocentre locations

An initial location, using HYPOINVERSE, of the identified and picked earthquakes returned 106 local earthquakes. The earthquakes cluster around the Leeu Gamka region in the same region as the previously identified cluster recorded by the National Seismic Network. The events recorded cluster in a surprisingly small area (75 % of the total

number of events recorded fall within a one square kilometre block) before relocation shown in Figure 4.2. The hypocentral depths are not well constrained at this point, but their apparent range puts them at the base of the Karoo basin when the Crust1.0 model is used for location.

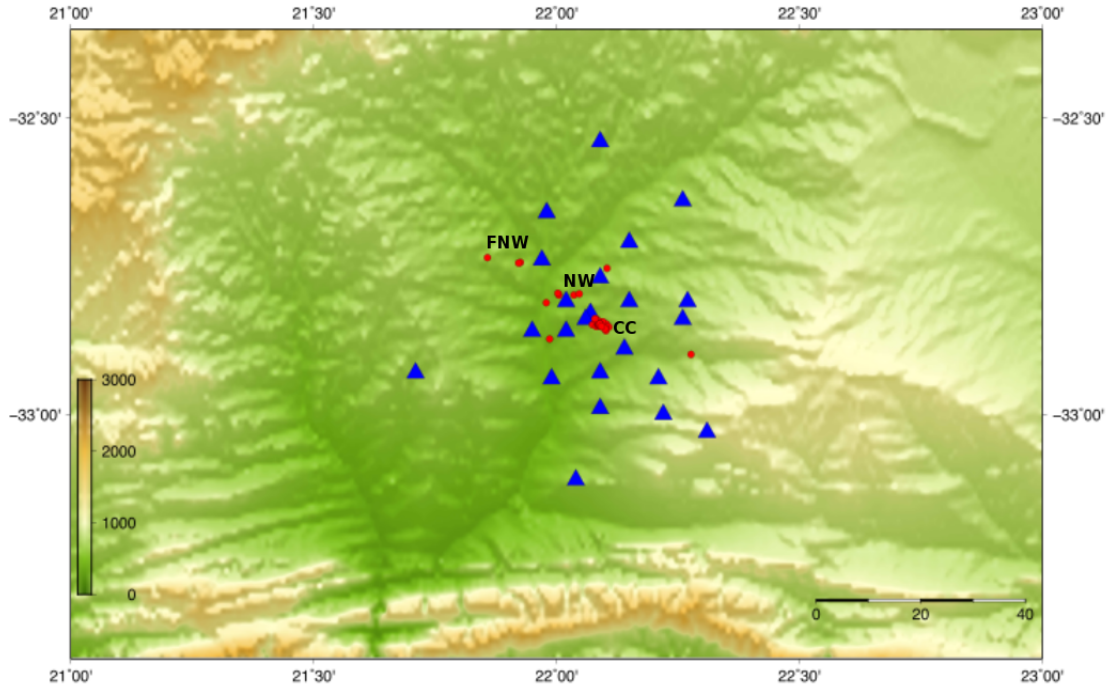

Figure 4.2: The station locations are plotted using the blue triangles and the earthquake locations are plotted using red circles.

The earthquakes were relocated using the hypocentral double-differencing technique, which resolved the earthquakes onto a NW – SE striking feature shown in Figure 4.3 and aligns with the general fabric of the satellite imagery shown in Figure 4.4. The final locations of the earthquakes using the SEISAN software as well as the relocated earthquakes using HYPODD are illustrated in Figure 4.3.

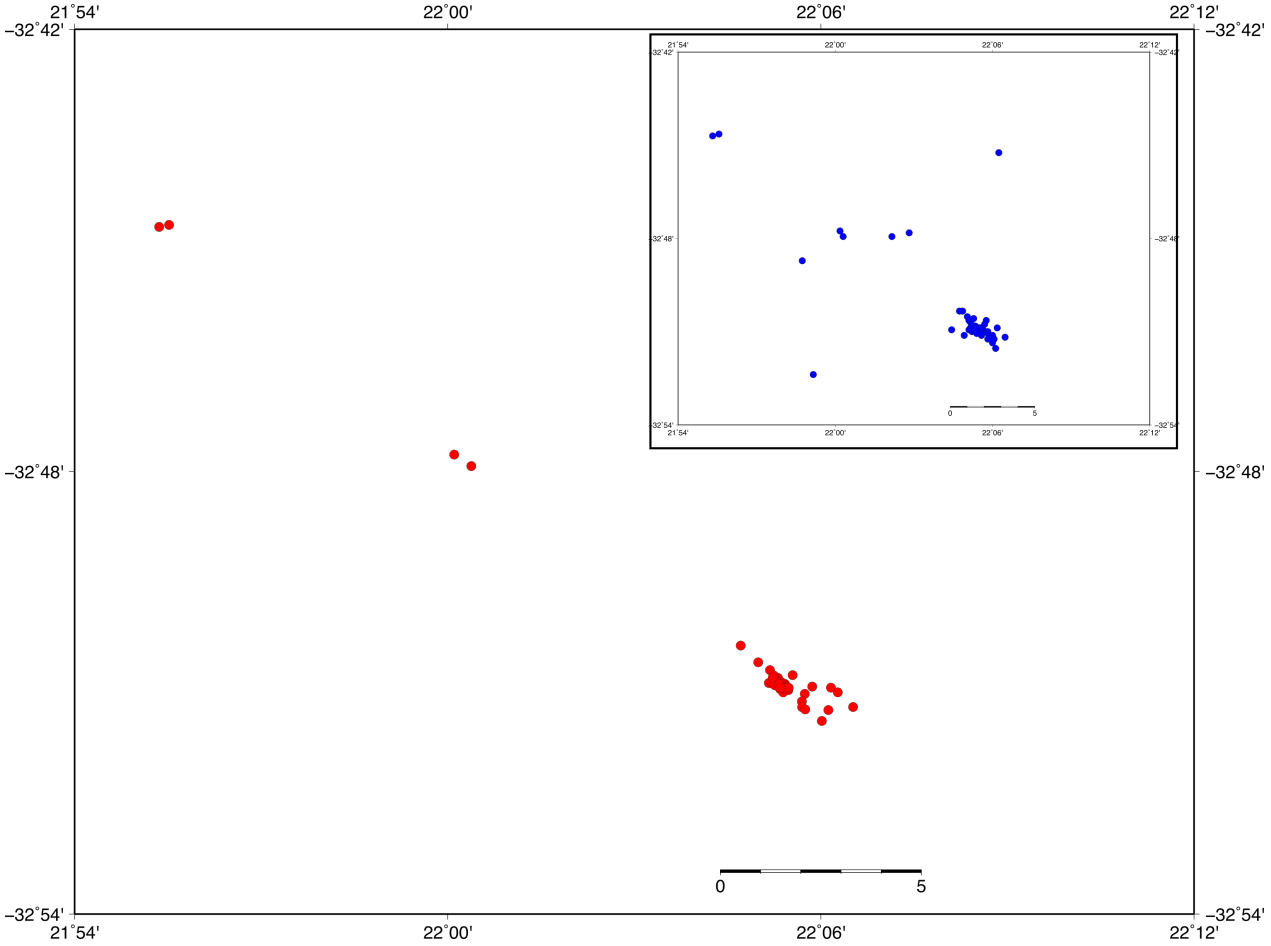

Figure 4.3: A map showing the original locations of the earthquakes represented as blue dots (inset) vs the relatively relocated earthquakes represented as red dots (main image) using the hypo double-differencing method.

The events clustered in time also appear to be clustered in space. There are three main clusters of events recorded during the deployment period. The main cluster (labelled CC in Figure 4.2) is found to the SE of Leeu Gamka, where 94 of the 106 local events were recorded. The second cluster lies to the the NW of this (labelled NW), and is the most central cluster. Only five events were recorded in this region at anomalous times during the three-month deployment, their depths range between 4.9 km and 6.8 km. A bit further to the NW another cluster of three events (labelled FNW) were recorded with approximate depths of 3.3 km - 3.7 km. A further four events were recorded and are randomly scattered throughout the study area. The waveforms of the events clustered

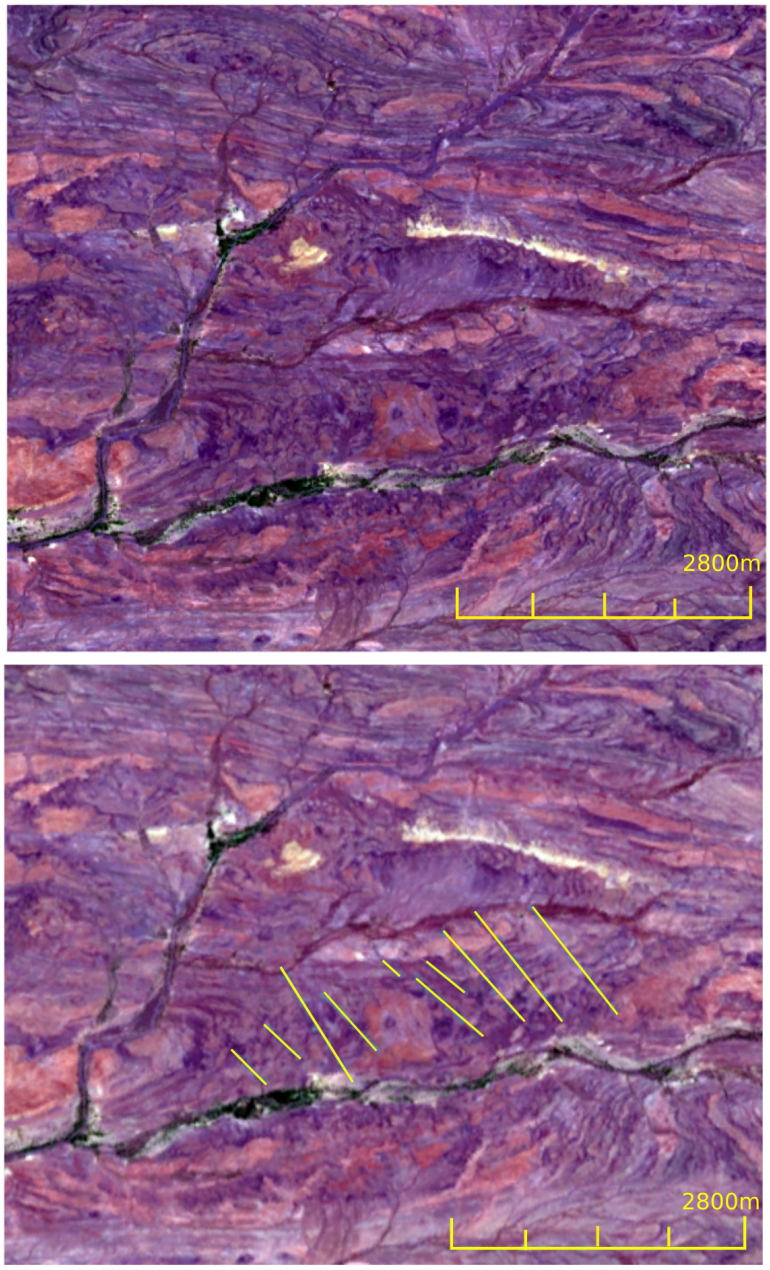

Figure 4.4: Satellite terrain imagery with 15m resolution (top) with a duplicated image (bottom) highlighting the NW – SE fabric, shown by the yellow lines, in the study area.

together, on the same day or closely in space, were analysed to check for similarities in the P- and S-wave arrivals and waveforms and will be discussed in section 4.5.1 on waveform similarities.

The 106 local earthquakes were recorded with measurable amplitudes, using the Wood-Anderson filter. This filter is designed to calibrate amplitudes for local networks. The earthquake magnitudes for earthquakes recorded in the Leeu Gamka region range randomly from M_{L}-1.5 to M_{L}0.4 without any clear relationship between earthquake magnitude and the time history of seismicity.

4.3 Earthquake depths

The earthquake depths were plotted with the locations obtained from HYPOINVERSE. The initial locations show that the depths increase on what appears to correspond to a sub-vertical structure between the longitudes of 22.07° and 22.10°. Frequency depth plots below in Figure 4.5 and 4.6 illustrate the depths at which the earthquakes commonly occur, assuming a chosen depth to the base of the Karoo basin. Assuming a reasonable thickness of the Karoo basin, based on previous studies and low residuals in the location of earthquakes using HYPOINVERSE, an average depth of the earthquakes can be determined. The deepest earthquake recorded located a depth of 11.4 km, assuming a Karoo thickness of 5 km. Shallow small earthquakes are typical of intraplate regions (Alabi et al., 2012).

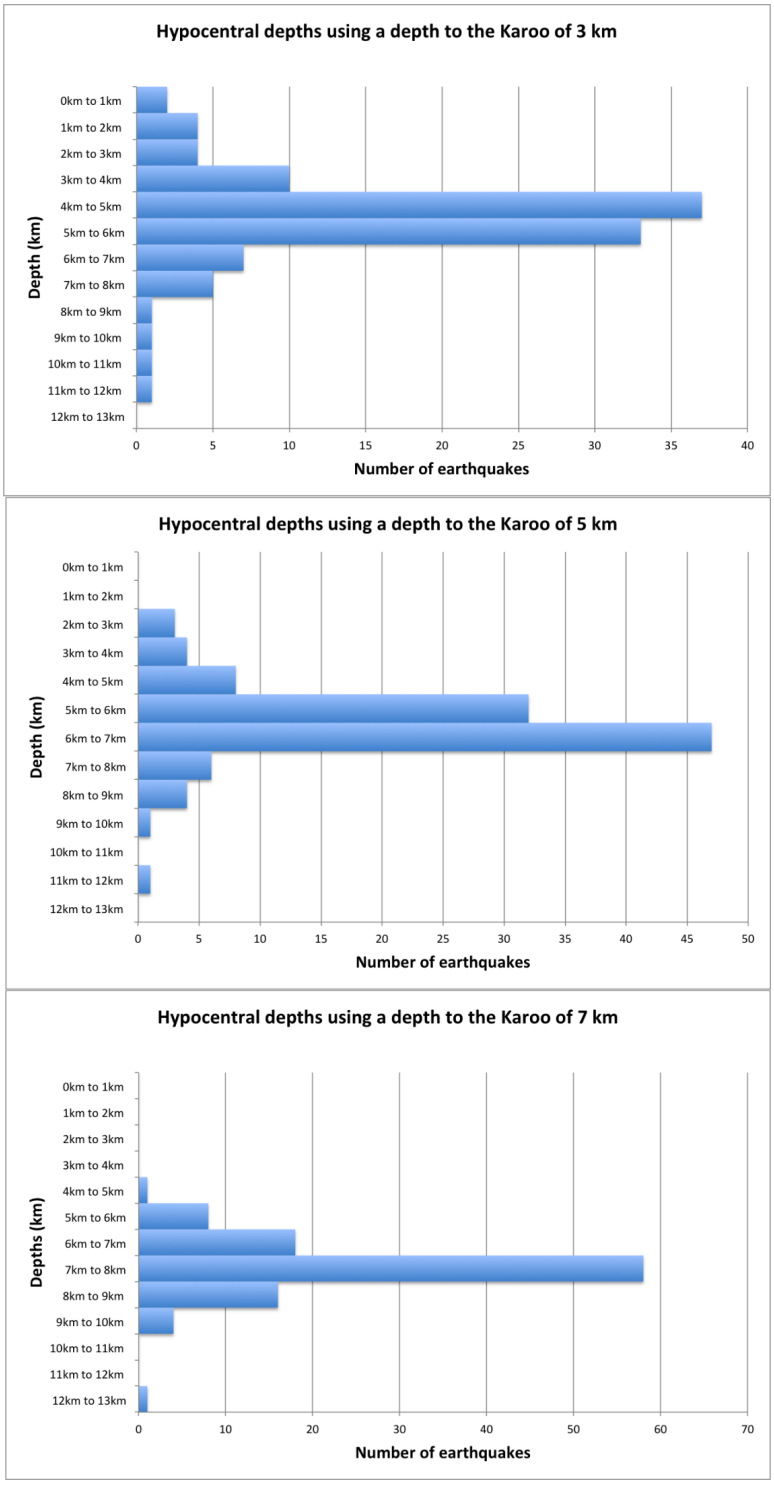

Figure 4.5: Depth variations of the hypocentres using Karoo thickness of 3 km, 5 km and 7 km.

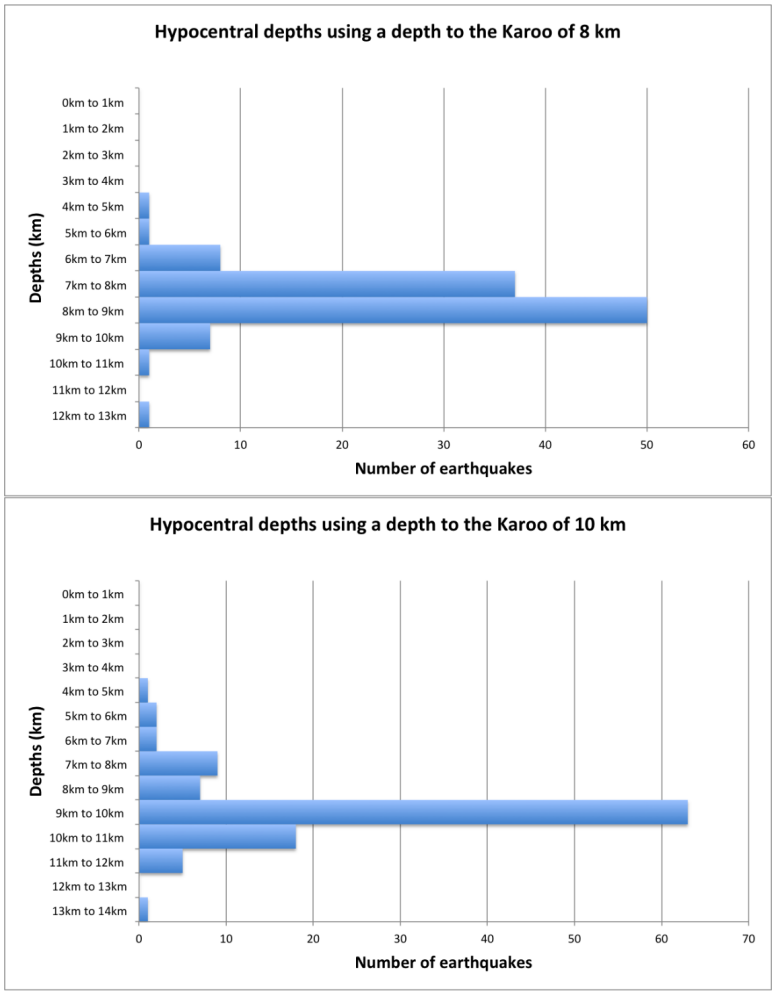

Figure 4.6: Depth variations of the hypocentral depths using a Karoo thickness of 8 km and 10 km.

The velocity model was tested by relocating the earthquakes using different lithological thicknesses and velocities and the best results (i.e. with the lowest residuals and most reasonable thicknesses) selected for the layers is tabulated in Table 4.1 below.

	Depth (km)
Sea level	-1
Top of Dwyka	2
Base of Karoo	4
	17.15
	32.92
MOHO	48.69
	60

Table 4.1: Table showing the velocity model used to calculate hypocentre location for the dataset with the lowest residuals and most reasonable lithology thicknesses based on the literature.

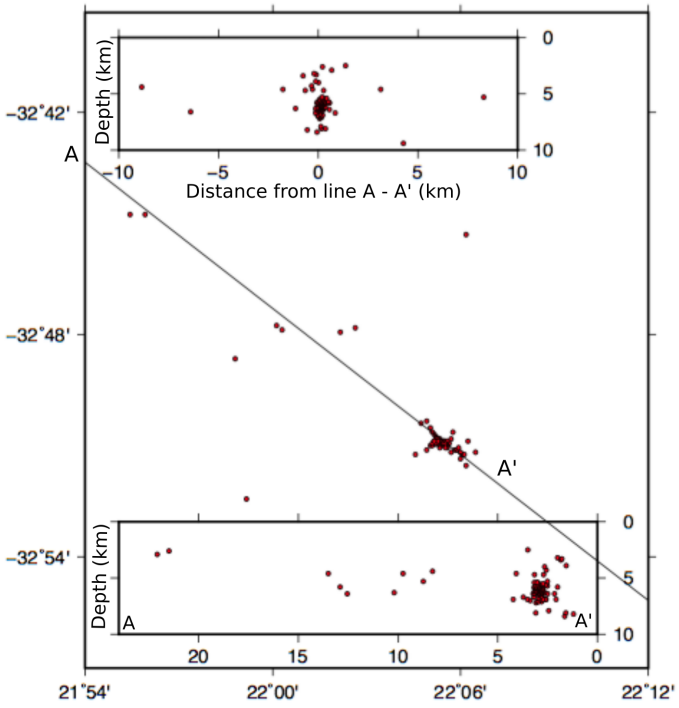

Figure 4.7: Depth projections along the line from A–A' (bottom) and depth variations with increasing distance away from the line A–A' (top).

Assuming a Karoo basin thickness of 5 km, we can say that the average depth of the earthquakes recorded during the study period locate between 6–7 km depth, placing them in the Cape Supergroup, just below the base of the Karoo. Unless an unreasonably

thick Karoo basin thickness is assumed, all the average earthquake depths locate within the Cape Supergroup. A Karoo thickness of 10 km will result in the average depth of the earthquakes predominantly locating within 9–10 km depth.

The average depth of the earthquake hypocentres, assuming a depth to the base of the Karoo of 5 km, is aproximately 6 km. The depths increase slightly to the east, however, at the cluster of earthquakes between 22.07° and 22.10° E, the earthquake depths vary but are mainly concentrated between 6–7 km deep. Figure 4.7 shows the depths projected onto a cross-section running from A–A' (bottom) and the depth variation from the central cluster away from the line A–A' (top).

4.3.1 Magnitude-frequency distribution

The M_c plot for the dataset shows that the small events between M_L0.1 and M_L-0.8 are well represented. Below M_L-0.8 the slope of the cumulative magnitude-frequency changes considerably as shown in Figure 4.8. Human induced activities close to farming activities may affect the accuracy of recording during the deployment period. A low signal-to-noise ratio on the seismograms, make identifying very small events difficult because of the small difference between background noise and signal produced by an event. A magnitude of completeness of M_L-0.8 and using a confidence of 90% we can say that the b-value lies between 1.23 and 2.07 shown in Figure 4.9. This is usually expressed by a change of the slope of the magnitude-frequency fit towards lower magnitudes. The minimum magnitude of completeness (M_c) can be defined as the minimum magnitude above which, all earthquakes in a certain region are reliably recorded (Shearer, 2009). This value will vary depending on the network and station recording capabilities, the short recording time period and therefore low number of recorded events.

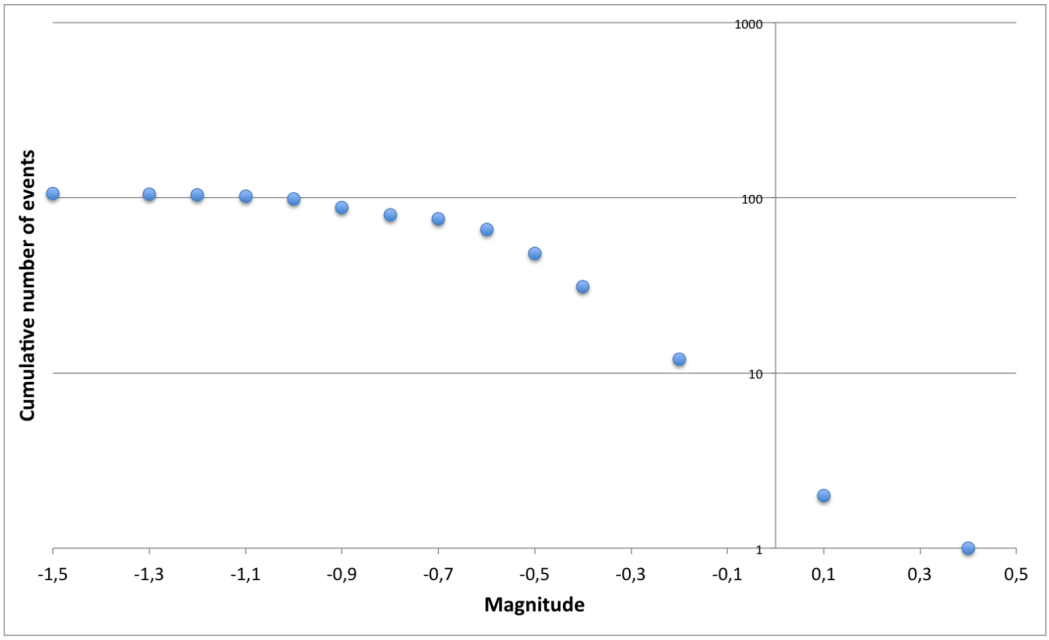

Figure 4.8: A Gutenberg-Richter plot showing the range of magnitude values recorded and the magnitude of completeness recorded.

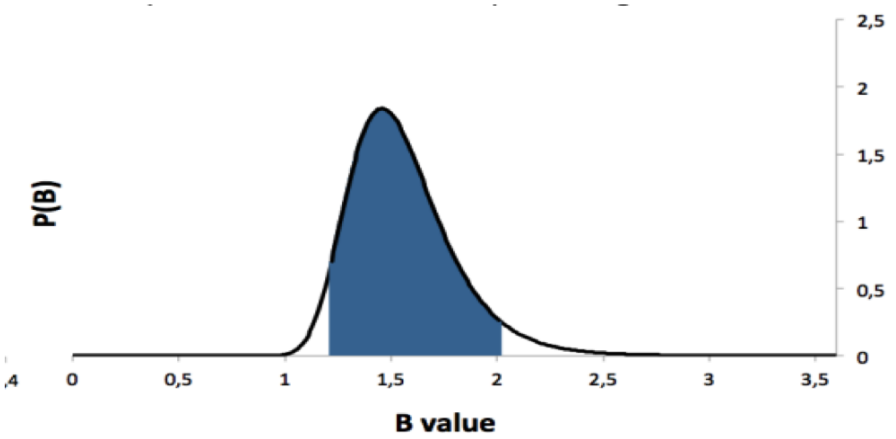

Figure 4.9: The 90% confidence of the b-value lies between 1.23 and 2.07 and is illustrated in the plot.

Focal Mechanisms						
Date	Time	Strike	Dip	Rake	Sites	Magnitude
20150318	3109	98	66	-50	21	-0,5
20150318	0518	94	73	-10	18	-0,6
20150318	0725	115	48	-6	19	-0,6
20150318	0728	111	66	-33	18	-0,9
20150318	0907	135	74	53	18	-0,4
20150318	2237	106	78	8	19	-1,0
20150323	1057	124	67	32	18	-1,2
20150325	1835	107	78	-22	20	-0,7
20150326	0802	151	33	62	20	-0,7
20150326	0804	108	68	5	20	-0,5
20150329	0046	106	68	-35	19	-0,5
20150329	0419	153	42	67	19	-0,8
20150421	0102	76	45	-45	18	-0,6
20150426	1725	157	88	-22	18	-0,6
20150504	0126	103	82	-18	18	-0,6
20150508	1507	114	76	-4	22	-0,2
20150519	0012	143	61	-22	18	-0,2
20150527	2103	133	89	-62	18	0,1

Table 4.2: The results of 18 focal mechanisms calculated for the study region.

4.4 Focal Mechanism statistics

The focal mechanisms for 18 of the local seismic events recorded by the network essentially have similar focal mechanisms as a result of them locating along the same structure in the same region. The dominant mechanism calculated in this study is strike-slip. A strike-slip focal mechanism, by definition, is described as two planes at right-angles to each other in space. Slip is possible on either plane, and this ambiguity is resolved by assuming the slip will occur along the plane in the same orientation as the distribution of events in the earthquake cluster (NW-SE). The results are summarised in the Table 4.2 and displayed in Figure 4.10.

The strike range for the focal mechanisms calculated vary between 76 ° - 157 °. In order to constrain the strike to the main structure in the area an average focal mechanism was calculated as will be discussed in the next section. The dominant mechanism has a fault plane striking WNW – ESE/NW – SE and only mechanisms that could possibly have been a result of a strike-slip fault were considered for this average.

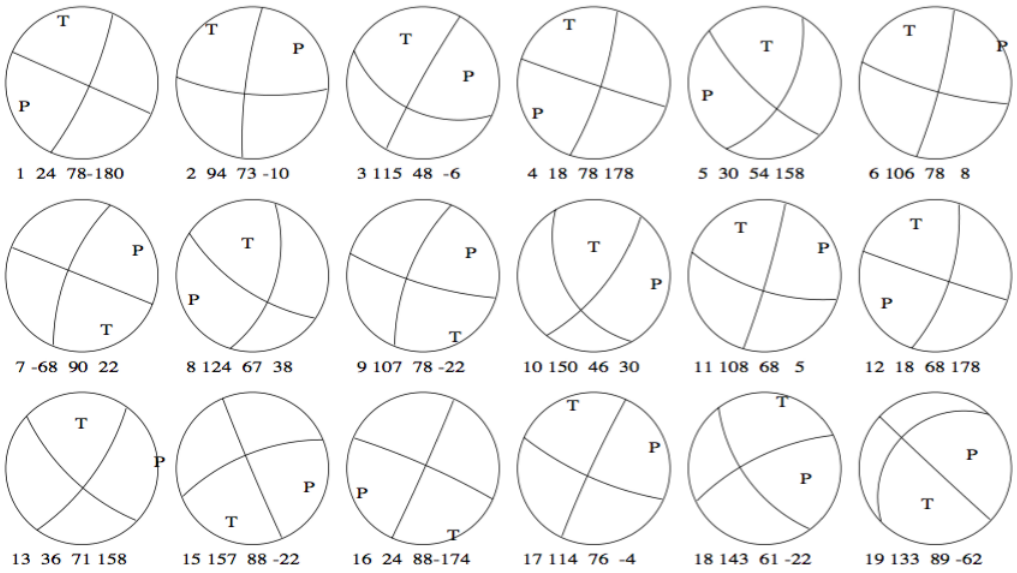

Figure 4.10: The focal mechanism calculated in SEISAN, for 18 selected events which triggered 18 or more stations. The focal mechanisms were calculated using the FOCMEC program in SEISAN (Snoke, 1984) which uses the polarities and station locations to determine the fault plane solution. The computed focal mechanisms shows only the P and T axis and do not use shading.

4.5 Average Focal Mechanism

An average moment tensor was calculated for the region and is described as the averaged representative seismic moment tensor characteristic of the study area. The average moment tensor is calculated for 10 micro-earthquakes with left-lateral, strike-slip focal mechanisms and were selected for this evaluation because it was the dominant mechanism observed and the result would be less reliable if events with mechanisms requiring a completely different fault is used. The station position and first motions in each quadrant are shown in Figure 4.11 and Figure 4.12 to demonstrate the azimuthal coverage and the certainty of the fault plane solution. The results of the average focal machanism produced focal mechanisms with a strike-slip mechanism of failure with an average strike, dip and rake of 105°, 73° and -18° respectively. (see Fig 4.13).

Focal Mechanisms						
Date	Time	Strike	Dip	Rake	Sites	Magnitude
20150318	0310	98	66	-50	21	-0,5
20150318	0518	94	73	-10	18	-0,6
20150318	0728	111	66	-33	18	-0,9
20150318	2237	106	78	8	19	-1.0
20150325	0018	107	78	-22	20	-0,7
20150326	0804	108	68	5	20	-0,5
20150329	0046	106	68	-35	19	-0,5
20150504	0126	103	82	-18	18	-0,6
20150508	1507	114	76	-4	22	-0,2

Table 4.3: Events used to calculate the average focal mechanism for the Leeu Gamka region

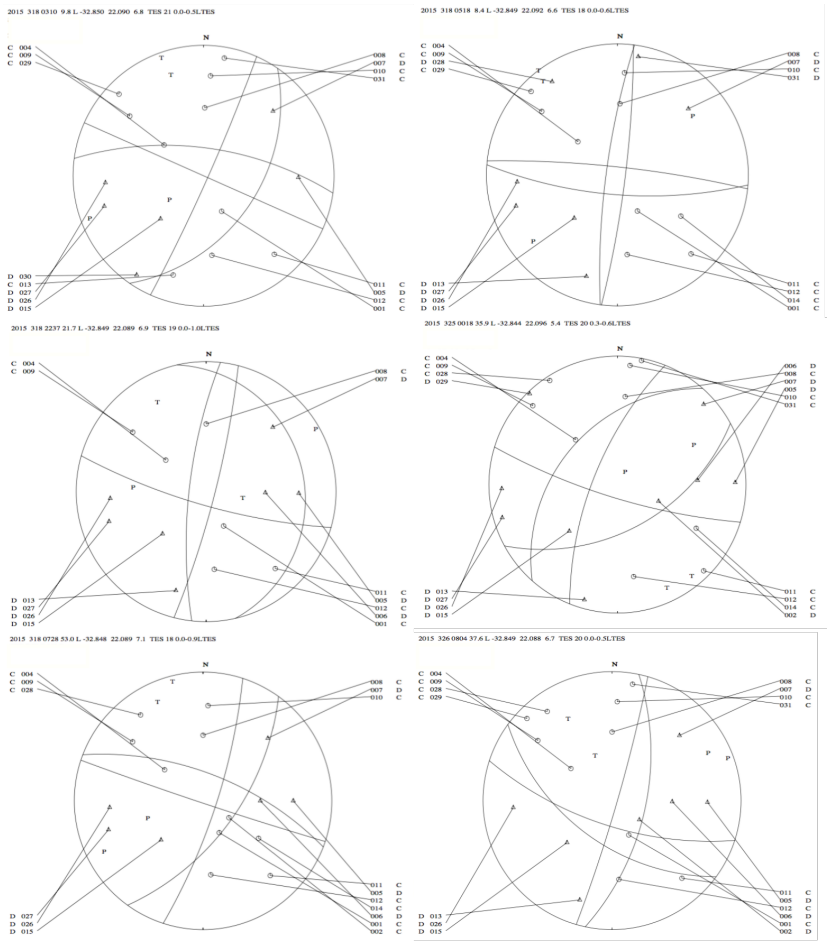

Figure 4.11: The focal mechanism solutions of six focal mechanisms to illustrate the station positions and polarities within each quadrant. Two solutions are represented in the plots, the strike-slip mechanism being the most stable in terms of first motions observed in the quadrants.

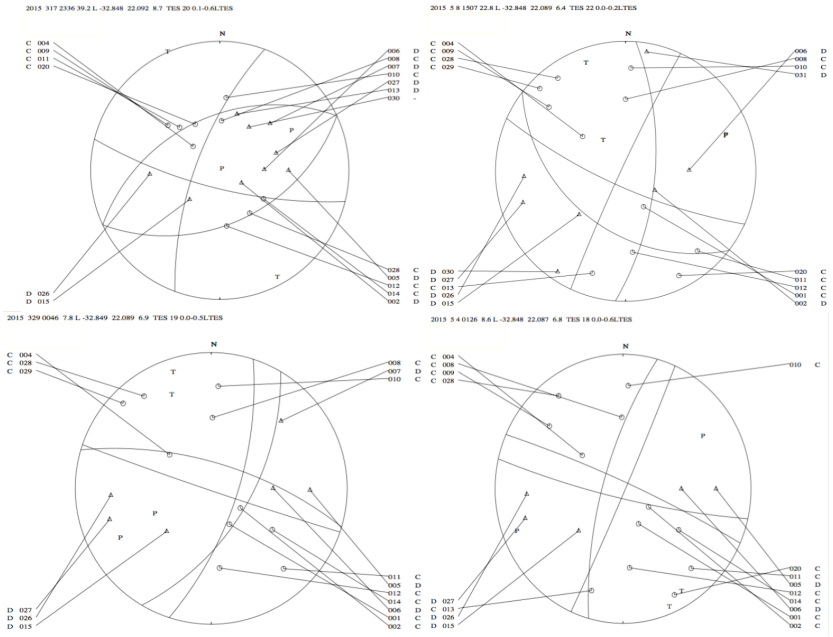

Figure 4.12: The focal mechanism solutions of four focal mechanisms to illustrate the station positions and polarities within each quadrant.

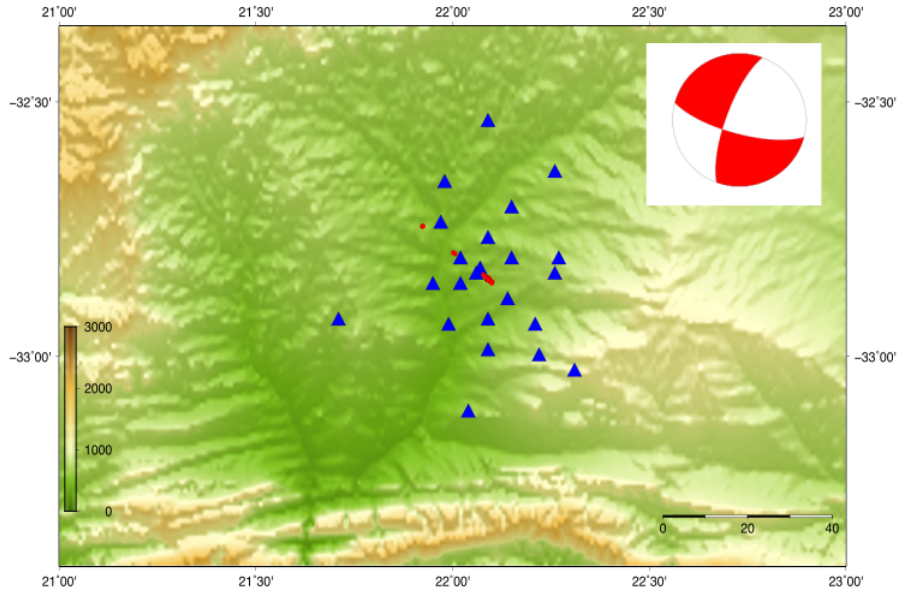

Figure 4.13: Represents the average solution of the calculated focal mechanisms of 10 of the 18 calculated focal mechanisms, showing a strike-slip mode of failure. The red (compressive first motion of the P-wave) quadrants contain the tension axis (T), which reflects the axis of maximum lengthening and the white quadrants (dilatational first motion of the P-wave) contain the pressure axis (P), which reflects the axis of maximum shortening

4.5.1 Waveform similarities

Looking at events recorded at common stations from a similar location, we expect that the waveforms should be similar. Three main clusters have been identified from the initial location of earthquakes, however relocation of these events show that the earthquakes relocate to a structure with a NW – SE orientation and all the relocated events locate on or near this structure, apart from five events. The waveforms of seven seismic events recorded in the central cluster were selected to observe the similarities in the waveforms. These events were time shifted to a common time and compared for seven events recorded at a common station and similar waveforms were observed, as seen in Figure 4.14.

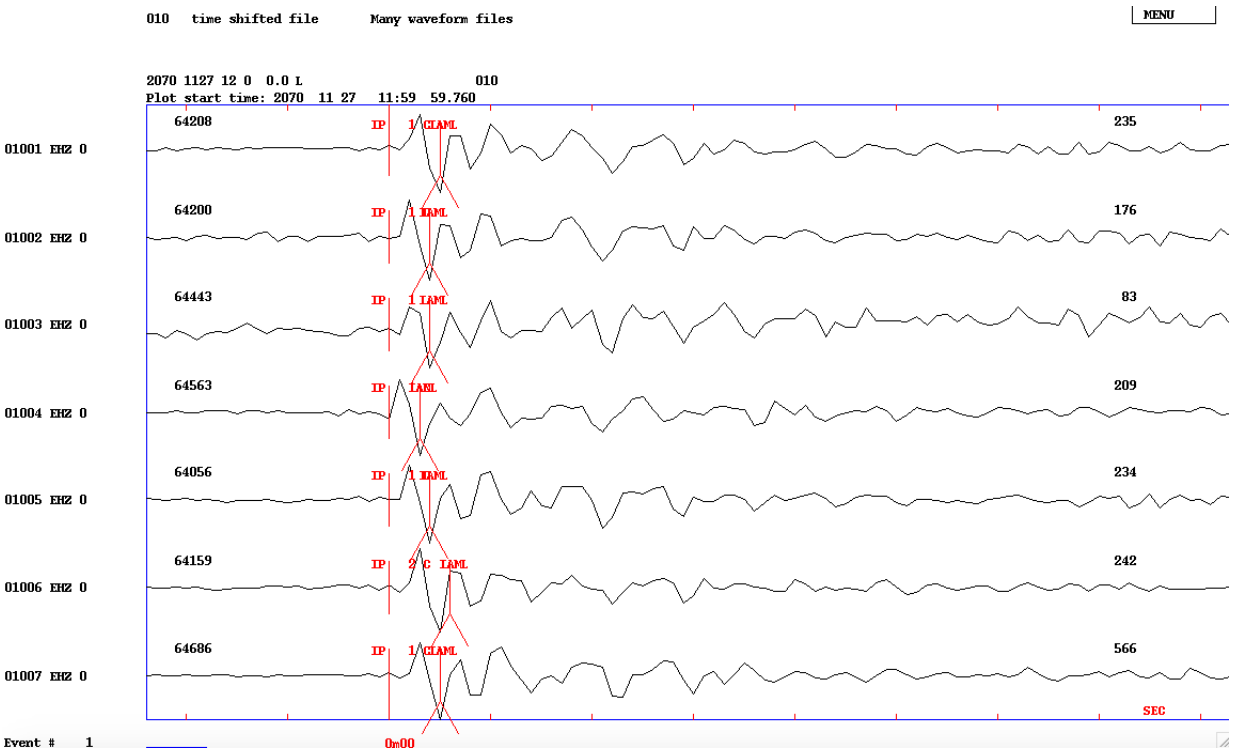

Figure 4.14: Figure showing the waveforms aligned to a common time from seven different earthquakes recorded at station 10. Each tick mark represents 0.1 seconds.

On visual inspection the waveforms, as expected, are similar. This suggests that it would be useful to perform a waveform cross-correlation of the events, from similar areas, recorded at the same station. However, this is not within the scope of work of this masters thesis and would be useful for further studies.

5 | Discussion

5.1 Time-history distribution and hypocentre locations

The earthquakes, recorded on the National Seismic Network, between 2007 – 2013 locate near the town of Leeu Gamka in a small cluster. The earthquakes appear to be clustered temporally, but it was established that the Council for Geoscience (CGS), who supplies seismic data recorded from the national seismic network to the ISC, stopped reporting data between 2013 – 2015. The cluster is therefore most likely an artefact of this. One of the aims of the project, amongst others, was to record seismicity in the region which previously recorded earthquakes and to locate their hypocentres and analyse the statistics related to the seismic events. 106 local earthquakes were recorded and picked over the duration of the deployment period and after manual processing of the seismic data, the earthquakes locate in the same region as the initial cluster recorded by the South African National Seismic Network. The depths of the earthquakes was an important research outcome, because the location with respect to the Karoo lithology will prove to be important in the event that hydraulic fracturing in the region commences, particularly if the wastewater produced is re-injected into the subsurface to a similar depth of the active fault. Pumping of fluids into a region that displays active faulting could result in an increase in the number of earthquakes recorded in the region or larger than expected earthquakes being recorded as observed in some regions of the United States, where the process of wastewater injection is being carried out. It should be noted that although the scope of the thesis looked at examples in the United States where hydraulic fracturing involved the process of re-injecting wastewater into the subsurface in order to dispose of

it, this might not necessarily be the only way to deal with the wastewater. The issue of waste water disposal could be the subject of a further study.

Testing the robustness of the velocity model and the effect of varying the thickness and velocities of the layers, is another important aim of the research. It was identified, from previous research and testing of the hypocentre locations, that the most appropriate velocity model consists of a Karoo depth at 5 km, resulting in the majority of the hypocentres plotting just below the contact of the Karoo and Cape Supergroups at a depth between 6–7 km. After testing a variety of thicknesses and velocities it was established that the hypocentre locations are not too sensitive when varying the parameters and ideally locate in the lithology below the Karoo basin, the Cape Supergroup. Only an unreasonably thin Karoo thickness in the velocity model would result in the hypocentres being forced into the Karoo basin (see more in section 5.2). A longer deployment period may have resulted in more earthquakes recorded with varying depths, making it possible to invert for a robust velocity model at the same time as the locations. This would constrain the velocities used in the model, making it more representative of the study region, particularly the velocities in the shallow regions of the model.

Relative relocation was performed on the 106 earthquakes using the program HYPODD. The relocated earthquakes align on a NW – SE striking feature and the deepest earthquake located is at 21 km. The parameters used for the relocation relocate 91 earthquakes out of the 106. The NW – SE striking feature has a similar orientation to faults mapped in other regions of the Western Cape. The depth of the deepest earthquake is assumed to be the depth of the seismogenic zone, at least for the time-scale of this study, and coincides with a depth that corresponds to just below the base of Karoo.

The earthquakes, particularly after relocation, align with a plane with a sub-vertical dip of approximately 73°, which does not appear to align with any previous mapped faults in the Leeu Gamka region but does align with the general fabric that can be seen in satellite imagery. The depth profile shows a sub-vertical structure between the longitudes 22.07 and 22.17 between 3 km – 12 km deep. The average depth of the seismic events recorded

during the deployment period appear to coincide with the depth just below the base of the Karoo, with the majority of the events recorded between 6-7 km depths.

The sporadic distribution of events during the deployment period is typical of a seismic swarm. According to Mogi (1967) a seismic swarm is defined as episodic sequences of a large number of seismic events that are clustered in space and time. They differ from the typical foreshock-mainshock-aftershock sequence, where the mainshock is usually followed by several low-magnitude earthquakes. A seismic swarm is generally not characterised by one large dominant event. This is the typical time-history of a swarm, characterised by a gradual increase in microseismic activity with alternating periods of low seismic activity (Van Noten et al., 2015). The largest events recorded during the deployment were recorded towards the end of May with another smaller swarm recorded between 17 and 27 May 2016. A $M_{\mathrm{L}}0.4$ earthquake was recorded on 24 May 2015 and a $M_{\mathrm{L}}0.1$ event was recorded on 27 May 2015. The micro-seismicity recorded during this period cannot be linked to any mainshock and this is confirmed by the ISC catalogue of earthquakes (recorded by the National Seismic Network) over this time period in this region, which does not show any events greater than $M_{\mathrm{L}}0.0$. The largest events were not recorded by the National Seismic Network and this is more than likely due to the sensitivity of the network to smaller events. Having a dense network of seismometers close to the epicentre of an earthquake swarm will record a large number of small earthquakes. Sometimes in an earthquake swarm, larger earthquakes may be recorded during the course of the seismic swarm but the many small events may not be linked to an identifiable mainshock (Van Noten et al., 2015).

This depth profile corresponds well with the focal mechanisms obtained for the majority of the micro-earthquakes recorded during the deployment period. For the depth of these earthquakes, a strike-slip mechanism is plausible as similar mechanisms have been observed in the Cape Supergroup in previous studies (Green and Bloch, 1971; Smit et al., 2015).

5.2 The velocity model

The hypocentre depths for individually located earthquakes will be affected by the velocity model chosen. The model chosen for this region is based on 7-layer model using the velocities calculated in the work carried out by Fatti (1987) and the CRUST1.0 model. The velocity model selected will affect the hypocentral depths calculated for the individually located earthquakes. The thickness of the individual layers and the velocities selected for the different lithologies. The more compacted the layer is the faster the V_p and V_s speeds will be. Generally, the velocities in the Karoo increase with depth, with the exception of the low velocity white marker band. The thicker the low velocity layer, the shallower the earthquakes will locate, whereas a thicker faster velocity layer will result in deeper earthquake locations. Thus, the velocity model chosen is vital in determining which lithology hosts the majority of the hypocentres, the Karoo Supergroup, Cape Supergroup or the basement rocks.

The sensitivity of the hypocentre locations to variations in the model was tested by using an unrealistically thin Karoo thickness of 3 km which would mean that the waves would travel faster from the source to the receiver on surface and have a small S-P distance because the slow velocity layer has been made thinner. In doing this we see that the earthquake depths are shallower than we expect and would place the hypocentres in the Karoo Basin. Making the Karoo thickness very thick, i.e 7 km – 10 km thick makes the slower velocity lithology thicker, meaning that the earthquakes would take longer to arrive at the receiver and a longer S-P distance, therefore placing the earthquakes very much deeper in the crust. The thickness of the Karoo, however is thicker than 3km and thinner than 7 km – 10 km, and from previous studies is shown to average between 5 km – 6 km over most of the Karoo. The results indicate that the earthquakes locate just below the base of the Karoo and one would have to vary the thickness quite significantly, using unreasonable thickness to have the earthquake hypocentres locate either in the Karoo or Basement rocks. I can say with some degree of confidence that assuming reasonable depths for the lithologies, we expect that the depths should be located approximately just

below the base of the Karoo sequence in the Cape Supergroup and it is then reasonable to assume that the earthquakes are a consequence of reactivation along a pre-existing fault.

5.3 Magnitude-frequency distribution

The b-value calculated for this data set is relatively high compared to that of b-values calculated for seismic swarms in other intraplate regions around the world (e.g. Hainzl and Fischer (2002); Ibs-von Seht and Klinge (2008); Van Noten et al. (2015). Previous studies have shown that individual structures or an individual fault delineated by earthquakes swarms can produce a robust Gutenberg-Richter relationship. This value suggests that this dataset has a higher proportion of smaller earthquakes than larger ones which have been observed in other intraplate regions. The data is in agreement with a study carried out by Andreoli et al. (2009) which analyses a set of data recorded by the SANSN. The b-value obtained for this data set was 1.23, very similar to the 90% confidence range of this dataset. It is important to note that a larger catalogue of data recorded over a longer duration of time would be more conclusive and that one cannot draw too many conclusions from such a short duration of data with respect to the magnitude of completeness and the b-value. Previous studies carried out in South Africa in the Western Cape region have achieved similar results with a larger dataset over a longer time period (Andreoli et al., 2009) who achieved similar results with a larger dataset.

5.4 Focal Mechanisms

The events are located in such close proximity to each other that it can be assumed that they share the same mechanism. This assumption was confirmed with the calculation of the focal mechanisms from the first motion polarities of waveforms from events recorded on 18 or more stations. Events used with the minimum number of observations or stations that recorded the event show a dominant average mechanisms with strike-slip solution

with a left-lateral sense of motion on the nodal plane (based on the orientation of the distribution of events during this deployment). This indicates, that in order to cause left-lateral motion and a dilational quadrant in the north-west, the P-axis would be in a east-west direction. These results are similar to the results obtained from studies in the Western Cape, in the Ceres-Tulbach region (Barth et al., 2008; Smit et al., 2015) and where a strike-slip mechanism with a NW-SE strike was observed for the events and general trend of seismicity. The results also correspond with the surface features observed in Google Earth Imagery where the average strike ranges between 115-125 degrees. The moment tensors mainly had similar focal mechanisms.

Previous studies in the study region studies show that a zone of compressive stress exists along the western coastal margin of South Africa, known as the Wegener Stress Anomaly (WSA) (Andreoli et al., 2009). The trend of this compressive stress is not well understood or clearly defined but strikes roughly NW-SE. In order to reactivate old structures, according to Andersonian theory, the angle between the greatest principle stress and the fault plane needs to be roughly 30 degrees. This is why although some faults may exist in these areas, they will not necessarily be activated due to the unfavourable orientation of the fault. The fault in the Leeu Gamka area is active and therefore must be reasonably oriented with respect to the greatest principle stress. This study, however, does not have enough focal mechanism observations in the surrounding areas to make a valid deduction about the principle stress in Leeu Gamka, however, stress measurements conducted further to the north-west of the region by (Viola et al., 2005) yielded the following results:

Stress measurements in the Carolusberg mine, Namaqualand, South Africa, yielded the following principal stress orientations and magnitudes:

- Σ_1: 40 MPa oriented NW/NNW
- Σ_2: 40 MPa oriented vertically
- Σ_3: 36MPa oriented SE/ESE (Viola et al., 2005)

These measurements illustrate that if the principle stress does not change drastically from the Carolusberg region to Leeu Gamka, a fault oriented NW or 30 degrees in either direction of the plane, is a plausible source for the earthquakes (according to Andersonian theory).

There are no mapped faults in the region and no obvious surface expressions of an active fault in the seismically active area. This however does not mean that there is no fault trace at the subsurface. What this study has revealed, is that there is an active fault in the region with a NW-SE striking surface, capable of generating an earthquake of $M_{\mathrm{L}}4.5$, the largest observed within the period between 2007 – 2013. The rocks exposed in this region belong to the Karoo Supergroup, more specifically the Abrahamskraal and Teekloof formations which are shales and mudstones which are easily weathered. The area is also a basin which has traces of paleorivers which were deposited as a thick succession of alluvium. The soft alluvium covers the in-situ rock making it difficult to see rock outcrop and therefore making it difficult to identify the fault trace on the surface. The seismicity, however, is localised on what appears to be a linear plane consistent with the nodal plane calculated by the focal mechanism.

5.5 Seismicity after deployment in Leeu Gamka

Eight earthquakes were recorded after deployment as shown in Figure 5.1. Reliable focal mechanisms of the earthquakes were not able to be determined by the CGS due to the event being recorded on a few very distant stations and the lack of clear arrivals on the seismograms. The biggest recorded event after the deployment was a M2.7 on 16 January 2017 at 01:50:24. It should be noted that the sensitivity of the national seismic network within the study area has an approximate location error of 3 – 4 km (Saunders et al., 2016). The earthquakes are likely to be associated with the fault identified in this thesis, but this cannot be concluded due to the sensitivity of the national seismic network.

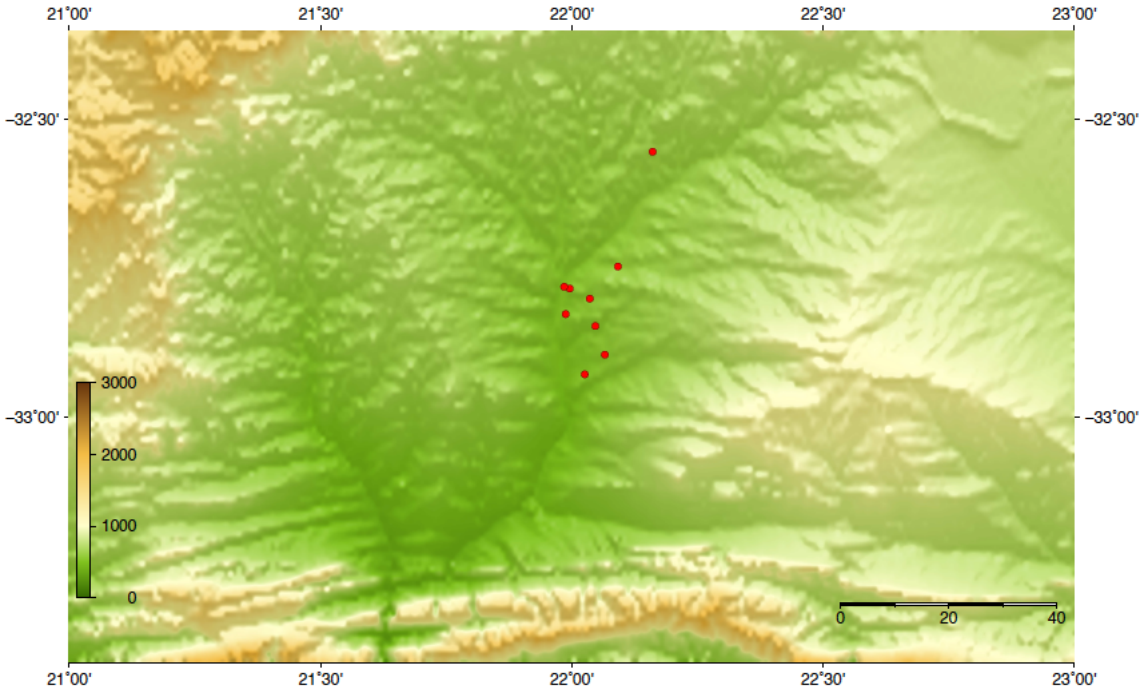

Figure 5.1: Seismicity after the deployment period of the Leeu Gamka array.

6 | Conclusions

Most of the seismicity recorded in South Africa is mining related, but occasionally, clusters like the Augrabies cluster in the northern Cape, the Drakensberg cluster, the Ceres-Tulbagh cluster and quite unexpectedly, the Leeu Gamka cluster, are observed and are of a tectonic origin. An anomalous cluster of earthquakes was identified in an intraplate region in Leeu Gamka in the Karoo. A dense array of seismometers was deployed over this cluster to study and analyse the detail of this seismicity. A total of 106 local earthquakes were identified and picked to understand their location, the source of the seismicity, the depth and orientation of the nodal planes of the source and what type of fault caused the seismic activity. This study is important because the area is currently being explored for shale gas, to be extracted by means of hydraulic fracturing. Significant evidence from previous studies suggest that the process of wastewater injection, part of the hydraulic fracturing process in the United States, has resulted in a significant increase in seismicity on faults that were not previously active and situated close to active wells or an increase in larger earthquakes than expected for that region. Providing a baseline study of seismicity and identifying active faults in a region being considered for shale gas extraction is vital. In this study the active part of the fault identified starts at a depth of approximately 6 km, a critically stressed zone within the Cape Supergroup, and could further be exacerbated by wastewater injection near this depth if this method is adopted for disposal. The wastewater produced by fracking merits further study.

An array of seismometers was deployed in a pattern that covered the previously observed events and a total of 106 local events were identified within the 65 km $\times$ 60 km boundary. The events were processed and located using both absolute and relative relocation meth-

ods. The events located within the same region as the previously reported seismicity, however the events appeared more clustered. Upon relative relocation of the events, the errors were minimised and the relative locations of the events improved. The relocated earthquakes locate on a linear feature, not previously identified by satellite imagery or previously mapped faults. The seismic events recorded in this study were not recorded by the national seismic network. In order to monitor seismicity in areas where deep injection wells are being considered a local network may need to be deployed accompanied by a microseismicity study similar to this thesis.

Previous geophysical studies have identified strong reflectors within the Karoo basin, which were used in this study to test and improve the velocity model used for locating the earthquakes in this region. Initially the Crust1.0 model was used, but it was realised that a more site specific model should be applied for the local cluster of earthquakes. The velocity model was tested by trial and error by varying the thicknesses of the lithologies, since all the earthquakes essentially located on one block in close proximity to each other, I assumed the velocity structure will be fairly homogenous in this area. Therefore, there was no need for station corrections, and a simple 7-layer 1-D model was selected, based on previous work by Fatti (1987), which had velocities ranging from Vp=4.9km/s at the surface to 6.4km/s. The Vp/Vs ratio was assumed to be 1.6 after tests were performed to check the average RMS and residual values after a location was performed. This model was observed to not be too sensitive to thickness variations. A thicker Karoo favoured deeper earthquake locations and a thinner Karoo favoured shallower locations. Several variations were tested and it was confirmed that as long as a reasonable velocity model is selected and a reasonable thickness for the Karoo basin was selected, the depths of the earthquakes preferentially locate just below the contact between the Karoo and Cape Supergroups.

The magnitude of the events ranged from -1.5 $< M_{\mathrm{L}} <$ 0.4 with a magnitude of completeness of M_c-0.8. The b-value calculated for this study is roughly 1.5, a high value but consistent with intraplate regions, which tend to have a higher b value as a consequence of the higher number of smaller events recorded, and the 90% confidence interval of the

b-values lie between 1.23 and 2.07. The calculated focal mechanisms in this region have a general NW – SE striking nodal plane, steeply dipping. This mechanism is consistent with mechanisms of larger events in the Western and Northern Cape close to the coast where the Wegner anomaly is said to be responsible for the NW-SE maximum horizontal compressive stress, which is typical of an Andersonian strike-slip regime. The mechanism estimated for the majority of well recorded events show a left-lateral sense of motion with a E-W dominant compressive stress. The fault is possibly activated by a lowering of the normal stress on the fault, by means of increasing the pore-pressure on the fault. The average depth of the hypocentres are in Cape Supergroup, a highly fractured quartzite aquifer, and the fault is possibly activated by an increase in pore-pressure at these depths associated with fluid flow.

Bibliography

Aki, K. (1967). Scaling law of seismic spectrum. *Journal of Geophysical Research*, 72(4):1217–1231.

Alabi, A. A., Akinyemi, O. D., and Adewale, A. (2012). Seismicity pattern in southern Africa from 1986 to 2009. *Earth Science Research*, 2(2):1.

Anderson, E. M. (1951). *The dynamics of faulting and dyke formation with applications to Britain*. Hafner Pub. Co.

Andreoli, M. A., Viola, G., Kounov, A., Scheepers, J., Heidbach, O., and Stengel, I. (2009). History of stress at Vaalputs, Namaqualand, South Africa: evidence for a Mid-Cretaceous "Wegener-type Orogeny" in western southern Africa. In *11th SAGA Biennial Technical Meeting and Exhibition*.

Barth, A., Reinecker, J., and Heidbach, O. (2008). Stress derivation from earthquake focal mechanisms. *World Stress Map Project Guidelines*, page 12.

Bordy, E. M., Hancox, P. J., and Rubidge, B. S. (2004). Basin development during the deposition of the Elliot formation (Late Triassic-Early Jurassic), Karoo Supergroup, South Africa. *South African Journal of Geology*, 107(3):397–412.

Bouchaala, F., Vavryčuk, V., and Fischer, T. (2013). Accuracy of the master-event and double-difference locations: synthetic tests and application to seismicity in west Bohemia, Czech Republic. *Journal of Seismology*, 17(3):841–859.

Brown, W. and Frohlich, C. Investigating the cause of the 17 May 2012 m 4.8 earthquake near Timpson, east Texas (abstr.). *Seismological Research Letters*.

Byerlee, J. D. (1966). *The frictional characteristics of Westerly granite.* PhD thesis, Massachusetts Institute of Technology.

Byerlee, J. D. and Brace, W. (1968). Stick slip, stable sliding, and earthquakes—effect of rock type, pressure, strain rate, and stiffness. *Journal of Geophysical Research*, 73(18):6031–6037.

Calais, E., Camelbeeck, T., Stein, S., Liu, M., and Craig, T. (2016). A new paradigm for large earthquakes in stable continental plate interiors. *Geophysical Research Letters*, 43(20):10,621–10,637.

Calais, E. and Stein, S. (2009). Time-variable deformation in the New Madrid seismic zone. *Science*, 323(5920):1442–1442.

Catuneanu, O., Hancox, P., and Rubidge, B. (1998). Reciprocal flexural behaviour and contrasting stratigraphies: a new basin development model for the Karoo retroarc foreland system, South Africa. *Basin Research*, 10(4):417–439.

Catuneanu, O., Wopfner, H., Eriksson, P., Cairncross, B., Rubidge, B., Smith, R., and Hancox, P. (2005). The Karoo basins of south-central Africa. *Journal of African Earth Sciences*, 43(1):211–253.

Craig, T., Jackson, J., Priestley, K., and McKenzie, D. (2011). Earthquake distribution patterns in Africa: their relationship to variations in lithospheric and geological structure, and their rheological implications. *Geophysical Journal International*, 185(1):403–434.

Davis, S. D. and Pennington, W. D. (1989). Induced seismic deformation in the Cogdell oil field of west Texas. *Bulletin of the Seismological Society of America*, 79(5):1477–1495.

De Wit, M. J. (2011). The great shale debate in the Karoo. *South African Journal of Science*, 107(7-8):02–10.

De Wit, M. J. and Ransome, I. G. (1992). Regional inversion tectonics along the southern margin of Gondwana. *Inversion Tectonics of the Cape Fold Belt, Karoo and Cretaceous Basins of southern Africa. Balkema, Rotterdam*, pages 15–21.

Delvaux, D. and Barth, A. (2010). African stress pattern from formal inversion of focal mechanism data. *Tectonophysics*, 482(1):105–128.

Ellsworth, W. L. (2013). Injection-induced earthquakes. *Science*, 341(6142):1225942.

Fatti, L. (1987). Reflection seismic surveys in the Karoo basin by Soekor. *SAGA Yearbook*, pages 22–30.

Frohlich, C., Ellsworth, W., Brown, W. A., Brunt, M., Luetgert, J., MacDonald, T., and Walter, S. (2014). The 17 May 2012 M4. 8 earthquake near Timpson, east Texas: An event possibly triggered by fluid injection. *Journal of Geophysical Research: Solid Earth*, 119(1):581–593.

Geel, C., De Wit, M., Booth, P., Schulz, H., and Horsfield, B. (2015). Palaeo-environment, diagenesis and characteristics of Permian black shales in the Lower Karoo Supergroup flanking the Cape Fold Belt near Jansenville, Eastern Cape, South Africa: Implications for the shale gas potential of the Karoo Basin. *South African Journal of Geology*, 118(3):249–274.

González, P. J., Tiampo, K. F., Palano, M., Cannavó, F., and Fernández, J. (2012). The 2011 Lorca earthquake slip distribution controlled by groundwater crustal unloading. *Nature Geoscience*, 5(11):821.

Green, R. and Bloch, S. (1971). The Ceres, South Africa, earthquake of September 29, 1969 I. Report on some aftershocks. *Bulletin of the Seismological Society of America*, 61(4):851–859.

Gutenberg, B. and Richter, C. F. (1944). Frequency of earthquakes in California. *Bulletin of the Seismological Society of America*, 34(4):185–188.

Gutenberg, B. and Richter, C. F. (1956). Earthquake magnitude, intensity, energy, and acceleration: (second paper). *Bulletin of the seismological society of America*, 46(2):105–145.

Hainzl, S. and Fischer, T. (2002). Indications for a successively triggered rupture growth

underlying the 2000 earthquake swarm in Vogtland/NW Bohemia. *Journal of Geophysical Research: Solid Earth*, 107(B12).

Hartnady, C. (2002). Earthquake hazard in Africa: perspectives on the Nubia-Somalia boundary: news and view. *South African Journal of Science*, 98(9-10):425–428.

Hartnady, C. J. (1990). Seismicity and plate boundary evolution in southeastern Africa. *South African Journal of Geology*, 93(3):473–484.

Havskov, J. and Ottemöller, L. (1999). Seisan: The earthquake analysis software, version 7.0: Inst. *Of Solid Earth Physics, Univ. of Bergen, Norway, 227pp.*

Hincks, T., Aspinall, W., Cooke, R., and Gernon, T. (2018). Oklahoma's induced seismicity strongly linked to wastewater injection depth. *Science*, 359(6381):1251–1255.

Horton, S. (2012). Disposal of hydrofracking waste fluid by injection into subsurface aquifers triggers earthquake swarm in central Arkansas with potential for damaging earthquake. *Seismological Research Letters*, 83(2):250–260.

Hubbert, M. K. and Rubey, W. W. (1959). Role of fluid pressure in mechanics of overthrust faulting I. Mechanics of fluid-filled porous solids and its application to overthrust faulting. *Geological Society of America Bulletin*, 70(2):115–166.

Ibs-von Seht, M., P. T. and Klinge, K. (2008). Earthquake swarms in continental rifts — a comparison of selected cases in America, Africa and Europe. *Tectonophysics*, 452:66–77.

Isacks, B., Oliver, J., and Sykes, L. R. (1968). Seismology and the new global tectonics. *Journal of Geophysical Research*, 73(18):5855–5899.

Jackson, J. (2001). Living with earthquakes: know your faults. *Journal of Earthquake Engineering*, 5(spec01):5–123.

Johnson, M., Van Vuuren, C., Visser, J., Cole, D., Wickens, H. d. V., Christie, A., Roberts, D., and Brandl, G. (2006). Sedimentary rocks of the Karoo Supergroup. *The Geology of South Africa*, pages 461–499.

Kanamori, H. and Anderson, D. L. (1975). Theoretical basis of some empirical relations in seismology. *Bulletin of the Seismological Society of America*, 65(5):1073–1095.

Kanamori, H. and Brodsky, E. E. (2004). The physics of earthquakes. *Reports on Progress in Physics*, 67(8):1429–1496.

Keranen, K. M., Savage, H. M., Abers, G. A., and Cochran, E. S. (2013). Potentially induced earthquakes in Oklahoma, USA: Links between wastewater injection and the 2011 Mw 5.7 earthquake sequence. *Geology*, 41(6):699–702.

Kim, W.-Y. (2013). Induced seismicity associated with fluid injection into a deep well in Youngstown, Ohio. *Journal of Geophysical Research: Solid Earth*, 118(7):3506–3518.

Kisslinger, C. (1980). Evaluation of S to P amplitude rations for determining focal mechanisms from regional network observations. *Bulletin of the Seismological Society of America*, 70(4):999–1014.

Klein, F. W. (1978). *Hypocenter locations program HYPOINVERSE*. US Department of the Interior, Geological Survey.

Krüger, F. and Scherbaum, F. (2014). The 29 September 1969, Ceres, South Africa, earthquake: Full waveform moment tensor inversion for point source and kinematic source parameters. *Bulletin of the Seismological Society of America*, 104(1):576–581.

Li, Q., Liu, M., and Stein, S. (2009). Spatiotemporal complexity of continental intraplate seismicity: insights from geodynamic modeling and implications for seismic hazard estimation. *Bulletin of the Seismological Society of America*, 99(1):52–60.

Lindeque, A., de Wit, M. J., Ryberg, T., Weber, M., and Chevallier, L. (2011). Deep crustal profile across the southern Karoo basin and Beattie Magnetic Anomaly, South Africa: an integrated interpretation with tectonic implications. *South African Journal of Geology*, 114(3-4):265–292.

Lindeque, A. S., Ryberg, T., Stankiewicz, J., Weber, M. H., and De Wit, M. J. (2007). Deep crustal seismic reflection experiment across the southern Karoo Basin, South Africa. *South African Journal of Geology*, 110(2-3):419–438.

Linzer, L., Bejaichund, M., Cichowicz, A., Durrheim, R., Goldbach, O., Kataka, M., Kijko, A., Milev, A., Saunders, I., Spottiswoode, S., et al. (2007). Recent research in seismology in South Africa. *South African Journal of Science*, 103(9-10):419–426.

Llenos, A. L., McGuire, J. J., and Ogata, Y. (2009). Modeling seismic swarms triggered by aseismic transients. *Earth and Planetary Science Letters*, 281(1-2):59–69.

Lomax, A., Michelini, A., and Curtis, A. (2007). Earthquake location, direct, global-search. In *Encyclopedia of Complexity and System Science*. Springer.

Malephane, H., Durrheim, R., and Andreoli, M. (2013). Seismic monitoring in Namaqualand/Bushmanland region. In *13th SAGA Biennial Conference & Exhibition*.

Manzunzu, B., Midzi, V., Mangongolo, A., and Essrich, F. (2017). The aftershock sequence of the 5 August 2014 Orkney earthquake (M L 5.5), South Africa. *Journal of Seismology*, 21(6):1323–1334.

McGarr, A., Bekins, B., Burkardt, N., Dewey, J., Earle, P., Ellsworth, W., Ge, S., Hickman, S., Holland, A., Majer, E., et al. (2015). Coping with earthquakes induced by fluid injection. *Science*, 347(6224):830–831.

McGarr, A., Simpson, D., Seeber, L., and Lee, W. (2002). Case histories of induced and triggered seismicity. *International Geophysics Series*, 81(A):647–664.

McNamara, D. E., Rubinstein, J. L., Myers, E., Smoczyk, G., Benz, H. M., Williams, R., Hayes, G., Wilson, D., Herrmann, R., McMahon, N. D., et al. (2015). Efforts to monitor and characterize the recent increasing seismicity in central Oklahoma. *The Leading Edge*, 34(6):628–639.

Midzi, V., Saunders, I., Brandt, M., and Molea, T. (2010). 1-D velocity model for use by the SANSN in earthquake location. *Seismological Research Letters*, 81(3):460–466.

Midzi, V., Zulu, B., Manzunzu, B., Mulabisana, T., Pule, T., Myendeki, S., and Gubela, W. (2015). Macroseismic survey of the ml5.5, 2014 Orkney earthquake. *Journal of Seismology*, 19(3):741–751.

Raleigh, C., Healy, J., and Bredehoeft, J. (1976). An experiment in earthquake control at Rangely, Colorado. *Science*, 191(4233):1230–1237.

Richter, C. F. (1935). An instrumental earthquake magnitude scale. *Bulletin of the Seismological Society of America*, 25(1):1–32.

Saunders, I., Kijko, A., and Fourie, C. (2016). Statistical evaluation of seismic event location accuracy by the South African National Seismograph Network over four decades. *South African Journal of Geology*, 119(1):291–304.

Saunders, I., Ottemöller, L., Brandt, M. B., and Fourie, C. J. (2013). Calibration of an ml scale for South Africa using tectonic earthquake data recorded by the South African National Seismograph Network: 2006 to 2009. *Journal of seismology*, 17(2):437–451.

Scheiber-Enslin, S. E. (2016). *Integrated geophysical investigation of the Karoo Basin, South Africa*. PhD thesis, Wits University.

Scholz, C. H., Aviles, C., and Wesnousky, S. G. (1986). Scaling differences between large interplate and intraplate earthquakes. *Bulletin of the Seismological Society of America*, 76(1):65–70.

Shearer, P. M. (2009). *Introduction to Seismology*. Cambridge University Press.

Sibson, R. (1992). Implications of fault-valve behaviour for rupture nucleation and recurrence. *Tectonophysics*, 211(1-4):283–293.

Singh, M., Kijko, A., and Durrheim, R. (2009). Seismotectonic models for South Africa: Synthesis of geoscientific information, problems, and the way forward. *Seismological Research Letters*, 80(1):71–80.

Smit, L., Fagereng, Å., Braeuer, B., and Stankiewicz, J. (2015). Microseismic activity and basement controls on an active intraplate strike-slip fault, Ceres–Tulbagh, South Africa. *Bulletin of the Seismological Society of America*, 105(3):1540–1547.

Smith, L. (2013). Microseismic observations in the Ceres-Tulbagh aftershock zone, Western Cape, South Africa, and their tectonic implications. Master's thesis, The University of Cape Town.

Snoke, J. (1984). A program for focal mechanism determination by combined use of polarity and SVP amplitude ratio data. *Earthquake Notes*, 55:15.

Spencer, B. (2008). Impact of earthquakes on the Central USA. Technical Report 08-02, Mid-America Earthquake Center, Urbana, Illinois.

Stankiewicz, J., Parsiegla, N., Ryberg, T., Gohl, K., Weckmann, U., Trumbull, R., and Weber, M. (2008). Crustal structure of the southern margin of the African continent: Results from geophysical experiments. *Journal of Geophysical Research: Solid Earth*, 113(B10).

Stankiewicz, J., Ryberg, T., Schulze, A., Lindeque, A., Weber, M., and De Wit, M. (2007). Initial results from wide-angle seismic refraction lines in the southern Cape. *South African Journal of Geology*, 110(2-3):407–418.

Talwani, P. and Gangopadhyay, A. (2003). Seismogenesis of intraplate earthquakes. In *Abst., Indo-US workshop on Seismicity & Geodynamics*, pages 16–17.

Tankard, A., Welsink, H., Aukes, P., Newton, R., and Stettler, E. (2012). Geodynamic interpretation of the Cape and the Karoo basins, South Africa. *Phanerozoic Passive Margins, Cratonic Basins and Global Tectonics Maps*, 869.

Thatcher, W. and C. Hanks, T. (1973). Source Parameters of Southern California Earthquakes. 78:8547–8576.

Van Bever Donker, M. A. J. (1996). Neotectonics of southern Africa - a review. *Africa Geoscience Review*, 3(1):1–16.

Van Noten, K., Lecocq, T., Shah, A. K., and Camelbeeck, T. (2015). Seismotectonic significance of the 2008–2010 Walloon Brabant seismic swarm in the Brabant Massif, Belgium. *Tectonophysics*, 656:20–38.

Vavryčuk, V. (2015). Inversion for the composite moment tensor. *Bulletin of the Seismological Society of America*, 105(6):3024–3035.

Viola, G., Andreoli, M., Ben-Avraham, Z., Stengel, I., and Reshef, M. (2005). Offshore mud volcanoes and onland faulting in southwestern Africa: neotectonic implications and constraints on the regional stress field. *Earth and Planetary Science Letters*, 231(1):147–160.

Waldhauser, F. and Ellsworth, W. L. (2000). A double-difference earthquake location algorithm: Method and application to the northern Hayward fault, California. *Bulletin of the Seismological Society of America*, 90(6):1353–1368.

Wang, C.-y. and Manga, M. (2014). Earthquakes and water. In *Encyclopedia of Complexity and Systems Science*, pages 1–38. Springer.

Wesson, R. L. and Nicholson, C. (1987). Earthquake hazard associated with deep well injection; a report to the us environmental protection agency. Technical report, US Geological Survey,.

7 Appendices

Earthquake data

Year	Month/Date	Time Hrs/Min	Seconds	Latitude	Longitude	Depth (km)	Magnitude	Strike	Rake	Dip
2015	3 6	2124	33.5	-32,812	21,979	5	-0,5			
2015	3 6	2244	29.1	-32,849	22,088	5,9	-0,5			
2015	3 7	857	1.9	-32,844	22,085	7,4	-1,5			
2015	3 8	1254	38.9	-32,848	22,09	6,8	-1,1			
2015	316	26	58.5	-32,796	22,003	6,9	-0,8			
2015	316	129	11.7	-32,799	22,036	6,3	-1,2			
2015	317	2336	40.1	-32,848	22,092	4,9	-0,6			
2015	317	2337	26.2	-32,849	22,09	6,6	-0,8			
2015	317	2341	52.3	-32,851	22,09	6,7	-0,4			
2015	317	2343	25.8	-32,849	22,092	6,5	-1,0			
2015	318	246	53.6	-32,852	22,1	5,8	-0,5			
2015	318	253	39.1	-32,848	22,091	6,9	-0,8			
2015	318	310	9.8	-32,85	22,09	6,8	-0,5	98	66	-50
2015	318	330	58.1	-32,849	22,091	6,8	-1,0			
2015	318	518	8.4	-32,849	22,092	6,6	-0,6	94	73	-10
2015	318	644	22.9	-32,848	22,089	6,4	1,1			
2015	318	716	15.3	-32,848	22,103	3	-1,1			
2015	318	725	44.3	-32,848	22,09	6,8	-0,6	115	48	-6
2015	318	727	34.7	-32,849	22,094	7	-1,1			
2015	318	728	53.0	-32,848	22,089	7	-0,9	111	66	-33
2015	318	746	13.2	-32,848	22,087	5,2	-1,2			
2015	318	749	25.0	-32,849	22,09	6,7	-1,0			
2015	318	906	54.9	-32,849	22,09	6,7	-0,8			
2015	318	907	7.6	-32,848	22,089	6,9	-0,4	135	74	53
2015	318	1104	32.2	-32,848	22,09	7,2	-0,9			
2015	318	1419	8.1	-32,849	22,089	7	-0,9			
2015	318	1956	24.6	-32,85	22,092	6,5	-1,0			
2015	318	2212	43.9	-32,849	22,088	6,3	-1,0			
2015	318	2236	15.4	-32,849	22,09	6,6	-1,1			
2015	318	2237	21.7	-32,849	22,089	6,9	-1,0	106	78	8
2015	319	623	20.7	-32,848	22,091	6,8	-0,8			
2015	319	1242	12.1	-32,847	22,088	7,8	-0,5			
2015	320	432	3.5	-32,848	22,089	6,8	-0,8			
2015	321	1639	43.7	-32,849	22,087	5,9	-0,9			
2015	321	2157	59.4	-32,848	22,088	6,6	-1,3			
2015	321	2228	11.1	-32,847	22,088	6,3	-1,1			
2015	323	1057	32.9	-32,849	22,089	6,7	-1,2	124	67	32
2015	323	2210	25.5	-32,848	22,088	6,4	-1,0			
2015	323	2230	7.4	-32,848	22,092	6,3	-1,1			
2015	323	2234	44.2	-32,849	22,086	6	-1,2			
2015	323	2240	15.8	-32,849	22,086	8,3	-1,2			
2015	323	2245	41.0	-32,849	22,09	7,4	-0,9			
2015	325	18	35.9	-32,844	22,096	5,4	-0,6	107	78	-22
2015	325	256	16.7	-32,847	22,087	6,4	-1,0			
2015	325	642	38.6	-32,849	22,089	6,6	-0,5			
2015	325	643	8.5	-32,848	22,093	6,8	-0,9			
2015	326	802	8.7	-32,848	22,089	6,8	-0,7	151	33	62
2015	326	802	48.8	-32,849	22,087	6,6	-0,8			

2015	326	804	37.6	-32,849	22,088	6,7	-0,5	108	68	5
2015	326	2114	44.2	-32,848	22,089	7	-0,9			
2015	326	2141	54.2	-32,848	22,087	6,2	-1,0			
2015	328	1104	8.2	-32,859	22,102	12,1	-1,0			
2015	328	1141	2.5	-32,848	22,087	6,5	-1,1			
2015	329	37	18.7	-32,849	22,088	6,8	-0,5			
2015	329	46	7.8	-32,849	22,089	6,9	-0,5	106	68	-35
2015	329	46	27.9	-32,849	22,086	6,6	-0,9			
2015	329	46	27.9	-32,849	22,085	6,6	-0,9			
2015	329	419	34.8	-32,849	22,09	6,7	-0,8	153	42	67
2015	329	1139	58.0	-32,849	22,089	6,3	-1,2			
2015	329	1145	57.1	-32,848	22,089	6,3	-1,1			
2015	329	1302	16.2	-32,843	22,088	7,2	-1,0			
2015	331	1519	27.8	-32,849	22,074	3	-1,2			
2015	331	1930	16.3	-32,849	22,091	6	-1,2			
2015	331	2007	37.7	-32,849	22,089	6,6	-0,9			
2015	331	2143	17.1	-32,849	22,086	6,1	-1,1			
2015	4 1	740	3.9	-32,85	22,087	6,1	-1,0			
2015	4 2	411	29.5	-32,849	22,088	6,4	-1,2			
2015	4 5	826	50.7	-32,852	22,082	7	-1,1			
2015	4 5	1239	50.6	-32,851	22,093	8,2	-0,9			
2015	4 5	2232	23.3	-32,848	22,088	6,7	-0,9			
2015	4 7	635	23.5	-32,848	22,09	7,2	-1,0			
2015	4 8	1727	36.7	-32,839	22,081	5,4	-1,0			
2015	4 9	2028	17.1	-32,797	22,047	5,1	-0,9			
2015	416	1707	50.0	-32,846	22,095	4,9	-1,1			

2015	417	1649	27.2	-32,854	22,1	2,4	-1,1			
2015	418	116	54.7	-32,848	22,086	6,9	-0,9			
2015	419	2331	45.0	-32,899	22,277	7,7	-0,8			
2015	421	102	44.6	-32,847	22,089	6,7	-0,6	76	45	-45
2015	421	128	37.6	-32,847	22,087	6,4	-1,0			
2015	426	1725	50.1	-32,854	22,101	9,6	-0,7	76	45	-45
2015	430	631	33.3	-32,845	22,086	7,4	-1,1			
2015	5 4	126	8.6	-32,848	22,087	6,8	-0,6	103	82	-18
2015	5 8	747	29.4	-32,848	22,089	6,6	-0,7			
2015	5 8	1507	22.8	-32,848	22,089	6,4	-0,2	114	76	-4
2015	513	1938	16.3	-32,754	22,104	4,9	-1,1			
2015	517	59	54.4	-32,854	22,097	7,8	-0,4			
2015	517	611	12.9	-32,848	22,088	7,5	-1,1			
2015	518	440	51.3	-32,848	22,088	7,5	-1,1			
2015	518	2209	19.5	-32,849	22,091	6,8	-0,9			
2015	519	12	52.4	-32,856	22,1	9,4	-0,2	143	61	-22
2015	519	228	37.0	-32,873	21,986	7,2	-0,6			
2015	520	2251	51.1	-32,849	22,092	7,5	-0,9			
2015	520	2252	7.4	-32,85	22,092	7,3	-0,8			
2015	522	1053	17.4	-32,853	22,108	8,8	-0,9			
2015	524	122	11.4	-32,852	22,093	8,4	0,4			
2015	524	422	9.7	-32,799	22,005	6,5	-1,0			
2015	524	1402	6.3	-32,847	22,088	6,8	-0,7			
2015	525	1525	34.6	-32,85	22,091	7,4	-0,9			
2015	526	451	46.0	-32,85	22,097	4,1	-1,1			
2015	526	451	45.8	-32,851	22,097	6,4	-1,1			

2015	526	2117	11.3	-32,839	22,079	7,7	-0,5			
2015	527	1158	57.6	-32,848	22,089	7,3	-1,2			
2015	527	1529	11.2	-32,842	22,084	7,1	-1,2			
2015	527	2103	28.3	-32,745	21,922	6,6	0,1	133	89	-62
2015	528	9	0.0	-32,736	21,858	11,7	-0,6			
2015	528	9	23.8	-32,744	21,926	6	-0,5			